Published in final edited form as:
J Med Chem. 2011 June 23; 54(12): 4018–4033. doi:10.1021/jm101591j.

Pyrimidine Nucleotides with 4-Alkyloxyimino and Terminal Tetraphosphate δ-Ester Modifications as Selective Agonists of the $P2Y_4$ Receptor

Hiroshi Maruoka[a], **M.P. Suresh Jayasekara**[a], **Matthew O. Barrett**[b], **Derek A. Franklin**[b], **Sonia de Castro**[a], **Nathaniel Kim**[a], **Stefano Costanzi**[c], **T. Kendall Harden**[b], and **Kenneth A. Jacobson**[a,*]

[a]Molecular Recognition Section, Laboratory of Bioorganic Chemistry, NIDDK, National Institutes of Health, Bethesda, Maryland 20892-0810

[b]Department of Pharmacology, University of North Carolina, School of Medicine, Chapel Hill, North Carolina 27599-7365

[c]Laboratory of Biological Modeling, NIDDK, National Institutes of Health, Bethesda, Maryland 20892

Abstract

$P2Y_2$ and $P2Y_4$ receptors are G protein-coupled receptors, activated by UTP and dinucleoside tetraphosphates, which are difficult to distinguish pharmacologically for lack of potent and selective ligands. We varied structurally phosphate and uracil moieties in analogues of pyrimidine nucleoside 5′-triphosphates and 5′-tetraphosphate esters. $P2Y_4$ receptor potency in phospholipase C stimulation in transfected 1321N1 human astrocytoma cells was enhanced in N^4-alkyloxycytidine derivatives. OH groups on a terminal δ-glucose phosphoester of uridine 5′-tetraphosphate were inverted or substituted with H or F to probe H-bonding effects. N^4-(Phenylpropoxy)-CTP **16** (MRS4062), Up_4-[1]3′-deoxy-3′-fluoroglucose **34** (MRS2927) and N^4-(phenylethoxy)-CTP **15** exhibit ≥10-fold selectivity for human $P2Y_4$ over $P2Y_2$ and $P2Y_6$ receptors (EC_{50} values 23, 62 and 73 nM, respectively). δ-3-Chlorophenyl phosphoester **21** of Up_4 activated $P2Y_2$ but not $P2Y_4$ receptor. Selected nucleotides tested for chemical and enzymatic stability were much more stable than UTP. Agonist docking at CXCR4-based $P2Y_2$ and $P2Y_4$ receptor models indicated greater steric tolerance of N^4-phenylpropoxy group at $P2Y_4$. Thus, distal structural changes modulate potency, selectivity, and stability of extended uridine tetraphosphate derivatives, and we report the first $P2Y_4$ receptor-selective agonists.

Keywords

G protein-coupled receptor; nucleotides; pyrimidines; phospholipase C; dinucleotide; cytidine

Introduction

The eight subtypes of P2Y receptors are nucleotide-activated G protein-coupled receptors (GPCRs), and four of these subtypes, the $P2Y_2$, $P2Y_4$, $P2Y_6$, and $P2Y_{14}$ receptors, respond

*Corresponding author: Laboratory of Bioorganic Chemistry, National Institutes of Diabetes and Digestive and Kidney Diseases, NIH, Bldg. 8A, Rm. B1A-19, Bethesda, MD 20892-0810, USA kajacobs@helix.nih.gov Phone: 301-496-9024. Fax: 301-480-8422.

Supplementary Material: NMR and mass spectra and HPLC traces for selected derivatives, x-ray structure of N^4-*t*-BuO-cytosine, and NOESY experiment are available.

to uracil nucleotides.[1,2] The $P2Y_2$ and $P2Y_4$ receptors are activated by uridine 5′-triphosphate (UTP, **1**, Chart 1) and its analogues and are difficult to distinguish pharmacologically, and a prominent need exists for definitive ligand tools.[3,4] The $P2Y_2$ receptor also is activated by analogues of adenine 5′-triphosphate.

Dinucleotide $P2Y_2$ receptor agonists, such as **2** (Up_4U, INS365), which are more resistant to enzymatic hydrolysis than **1**, are being developed clinically for treatment of eye and pulmonary diseases.[5–7] Compounds **1** and **2** are not selective for the $P2Y_2$ receptor. However, several studies have explored the structure activity relationship (SAR) of agonists[8, 9–13] and antagonists[14] at the $P2Y_2$ receptor, and potent and selective $P2Y_2$ receptor agonists, such as **4** (MRS2698)[10] and C-linked nucleotides[9] have been identified. The nucleotide agonists **5** – **7** also are $P2Y_2$ receptor-selective relative to both $P2Y_4$ and $P2Y_6$ receptors.[13] In contrast, the 2′-azido analogue **3** is one of the few analogues of **1** that displays any selectivity (only 5-fold in comparison to the $P2Y_2$ receptor) for the $P2Y_4$ receptor.[8] There are no selective antagonists of the $P2Y_4$ receptor.

In the present study, we further investigated SARs at the $P2Y_2$ and $P2Y_4$ receptors through synthesis of nucleotides with additional substitutions of the uracil and phosphate moieties and combinations thereof. These novel derivatives incorporated groups such as 4-methoxyimino and its homologues on the pyrimidine ring, found previously to enhance the potency of analogues of uridine 5′-diphosphate (UDP) at P2Y receptors.[15] We also probed the effects of substituting one uridine moiety of **2** with various sugar and aliphatic and aromatic alcohol moieties. Two lead δ -phosphoesters of 5′-tetraphosphates that were recently reported as full agonists of the $P2Y_2$ receptor,[13] i.e. **7** (MRS2768), which was $P2Y_2$ receptor-specific, and **8** (MRS2732), with 7- and 26-fold selectivity in comparison to $P2Y_4$ and $P2Y_6$ receptors, were modified in the present study. Although $P2Y_2$ receptor selectivity was not improved by these changes, several analogues exhibited important increases in potency and selectivity at the $P2Y_4$ receptor. This new chemical synthesis was combined with molecular docking studies based on a model derived from the recently solved structure of the CXCR4 chemokine receptor[16] to interrogate the molecular basis for selectivity of interaction of several of these molecules for the $P2Y_4$ receptor over the $P2Y_2$ receptor.

Results

Chemical Synthesis

Novel nucleotide derivatives (Tables 1) were prepared by the synthetic routes shown in Schemes 1 – 6. The potencies of nine known reference compounds (**1, 6–9, 17–19** and **27**) are also listed in Table 1.[11–13] The types of nucleotide modifications made included: analogues of cytidine 5′ -triphosphate (CTP) containing a N^4-alkoxy group (Scheme 1); 5′-tetraphosphates derivatives of **17** (Up_4) containing a substituted δ-phenyl phosphoester group at the terminal phosphate (Scheme 2 and 5); derivatives of **17** containing a sugar group at the terminal phosphate (Scheme 3 and 6); analogues of **1** containing a β,γ-dichloromethylene-bridge in the triphosphate group (Scheme 4).

The synthesis of N^4 -alkoxy cytidines **39** – **42** from cytidine was performed using corresponding alkoxy amines. The resulting N^4 -alkoxy cytidines were phosphorylated by standard methods[6] to give the desired N^4 -alkoxy-CTP analogues **11** – **16** (Scheme 1). In each case, the unprotected nucleoside was first treated with phosphorous oxychloride, and the reaction mixture was treated immediately with bis(tri-*n*-butylammonium) pyrophosphate to produce the 5′-triphosphate. The favored method for preparation of the β, γ-dichloromethylene derivative **10** was by condensation of dichloromethylenediphosphonic acid with uridine-5′-monophosphate (UMP) using *N*,*N*′-diisopropylcarbodiimide (DIC). An

alternate method involving reaction with UMP-morpholide required two weeks of reaction to reach completion.

The synthesis of 5′-tetraphosphate derivatives that were modified at the terminal phosphates was performed using a carbodiimide coupling reagent in the presence of magnesium chloride (Schemes 5 and 6). The addition of $MgCl_2$ dramatically increased the reactivity during the coupling reaction of monophosphate and triphosphate,[17] but it impeded the coupling of monophosphate and diphosphate (data not shown). Phenyl monophosphates **57** – **62** were prepared by phosphorylation with a dibenzyl-protected phosphate group followed by deprotection of the benzyl groups using trimethylsilyl bromide (TMS-Br, Scheme 2).[15] Hexose sugar monophosphates **68** – **72** were phosphorylated at the 1′-position by full acetylation and treatment with phosphoric acid. The synthesis of glucuronic acid-1-monophosphate **74** was performed by oxidation of commercially available glucose-1-monophosphate using 2,2,6,6-tetramethylpiperidine-1-oxyl (TEMPO) as a catalyst.[18]

Pharmacological Activity

Activation of phospholipase C (PLC) by a range of concentrations of each newly synthesized nucleotide derivative (**10** – **37**) was studied in [^{3}H]inositol-labeled 1321N1 human astrocytoma cells stably expressing the human $P2Y_2$, $P2Y_4$, or $P2Y_6$ receptor by following methodology (see Experimental Section) we described previously in detail.[13,15,19]

Table 1 illustrates analogues of **1** and **17** that were designed for possible interaction with the $P2Y_2$ and $P2Y_4$ receptors and their biological potencies. Introduction of β,γ-phosphonomethylene bridges, which enhances stability of nucleotides against the action of ectonucleotidases, resulted in compounds **6** and **10** that were inactive at the $P2Y_4$ receptor.[13]

The possibility of a hydrophobic pocket beyond the 4 position of the pyrimidine ring in the $P2Y_2$ or $P2Y_4$ receptor structure was probed in analogues of **1** with N^4-alkoxyimino moieties **11** – **16**. One of these molecules, N^4-methoxy-CTP **11**,[15] was more potent than the native ligand **1** at both subtypes. Within a related series of homologous arylalkoxy derivatives, the N^4-phenylpropoxy substitution of CTP in **16** was found to optimally increase activity at the $P2Y_4$ receptor with an EC_{50} value of 23 nM (Figures 1 and 2). This compound displayed selectivities of 28-fold and 32-fold in comparison to the $P2Y_2$ and $P2Y_6$ receptors, respectively. N^4-Phenylethoxy substitution of CTP resulted in a molecule **15** that exhibited somewhat lower potency (EC_{50} = 73 nM) and selectivity (16-fold and 17-fold in comparison to the $P2Y_2$ and $P2Y_6$ receptors, respectively) than **16** for the $P2Y_4$ receptor.

Introduction of either a sugar moiety or a substituted phenyl ring at the terminal δ-phosphate was examined in the series of 5′-tetraphosphates. We previously reported that introduction of a glucose or phenyl ester group at the δ-phosphate resulted in increased selectivity for the $P2Y_2$ receptor against the $P2Y_4$ and $P2Y_6$ receptors.[13] A 3-Cl derivative **21** showed higher potency than the phenyl derivative **7**, but its $P2Y_2$ receptor selectivity in comparison to the $P2Y_6$ receptor was decreased. Similarly, all substitutions of the δ-phenyl ester examined (**20** – **25**) were either less potent or less selective for the $P2Y_2$ receptor than the unsubstituted **7**.

Consistent with previous findings, introduction of a β,γ-dichloromethylene substitution in **24** abolished activity at the three P2Y receptors tested. Based on the $P2Y_2$ receptor selectivity of Up_4-δ-[1]glucose **8**,[13] substitutions of the δ -glucose moiety were examined (**26** – **37**). The types of glucose modifications included were inversion of hydroxyl groups (**27** – **29**), replacement of a hydroxyl group with F (**33** – **37**), and other omission or other replacement of hydroxyl functionality (**30** – **32**). These modifications resulted in greatly varied potency and selectivity for the P2Y receptors. Inversion of the 3′-hydroxyl group in the allose

derivative **28** increased $P2Y_4$ receptor potency 11-fold, but inversion of the 2′-hydroxyl group in the mannose derivative **29** decreased potency at $P2Y_2$, $P2Y_4$, and $P2Y_6$ receptors. Fluoro substitution at the 2′ position of the terminal δ-glucose moiety in **33** greatly reduced activity at all three receptor subtypes, suggesting that the H-bond-donating property of the 2′-hydroxyl group is necessary for this biological activity. The hydroxymethylene group appeared to be important for activity at the $P2Y_2$ receptor, because the xylose derivative **30** exhibited reduced activity (9-fold less potent than **8**) at this subtype.

The 3′- and 4′-fluoro derivatives **34** and **37** maintained activity at the $P2Y_2$ receptor. However, fluoro substitution at the 3′ position of the terminal glucose moiety in **34** greatly increased potency (EC_{50} = 62 nM) at the $P2Y_4$ receptor. Thus, $P2Y_4$ receptor selectivities of 11.5-fold and 15.3-fold were observed for this analogue in comparison to the $P2Y_2$ and $P2Y_6$ receptors, respectively. Analogues **35** and **36** that included combination of 3′-deoxy-3′-fluoroglucose with the N^4-benzyloxyimino or N^4-methoxyimino modification in the nucleobase were less active and selective than unmodified **34**. Thus, simultaneous introduction of these two $P2Y_4$ receptor-directing modifications did not produce further enhancement of potency or selectivity.

Molecular Modeling

In light of the SAR data generated through this work, in particular the different selectivity profile of compounds **11** and **16**, we revised our experimentally supported modeling hypothesis for the binding model of pyrimidine-based nucleotides to the $P2Y_2$ and $P2Y_4$ receptors, through the incorporation of further experimental data. These new models were not used to design the compounds but to offer a putative structural interpretation of the results. Note: to facilitate the comparison among receptors, throughout this section amino acid residues are designated both with their residue number in the $P2Y_2$ and $P2Y_4$ sequence as well as the universal GPCR residue identifier defined by the Ballesteros and Weinstein.[20,28,29]

In the absence of experimentally elucidated structures of any of the members of the P2Y family, in the last decade we have constructed models of the $P2Y_2$ and $P2Y_4$ receptors through homology modeling based on rhodopsin, which, at the time, was the only crystallographically solved GPCR, followed by molecular docking.[8,10,20] We incorporated into the models several hypotheses derived from experiments. These included the presence of two disulfide bridges and a salt bridge that putatively contribute to the shape of the extracellular domains of the receptors. Data from mutagenesis studies revealed that the residues involved in formation of these extracellular bridges are fundamental to the function of P2Y receptors.[22–24] The binding mode of the ligand was also driven by mutagenesis and SAR data. Specifically, our published models were constructed using as anchors for the binding of the phosphate moieties of the nucleotides three cationic residues located in TM3, TM6, and TM7 that are essential for ligand recognition according to mutagenesis data.[24–26] The Northern (N) conformation adopted by the ribose moiety of **1** and the orientation of the nucleobase toward the opening of the interhelical cavity are also supported by SAR data.[11,15,21]

Our rhodopsin-based models do not explain the different selectivity profiles of compounds **11** and **16**, because in those models the area that surrounds the N^4-substituents of the two compounds is completely conserved between the $P2Y_2$ and $P2Y_4$ receptors (Figure 3). Here, we propose revised models of the $P2Y_2$ and $P2Y_4$ receptors that incorporate the experimentally supported features of the previous models and are consistent with SAR data gathered in this work. The new models are based on the recently solved x-ray crystal structure of the CXCR4 chemokine receptor,[16] which, among all those currently available, is the closest to the P2Y receptors.[20] Among the crystallographically solved GPCRs, this

receptor shares the highest sequence similarity with P2Y receptors, showing 24.6% and 25.7% of sequence identity with the $P2Y_2$ and the $P2Y_4$ receptor – the sequence identity was calculated according to the alignment shown in Figure 4 and refers to the entire portion of the CXCR4 receptor that was solved crystallographically, with the exclusion of the C-terminal domain. Moreover, the CXCR4 contains a disulfide bridge, putatively present also in the $P2Y_2$ and $P2Y_4$ receptors, connecting the N-terminus (through a Cys located two positions upstream when compared to the P2Ys) with the boundary between EL3 and TM7 (through a Cys located at position 7.25, as in the P2Y receptors) – see Figure 4. Before the solution of the CXCR4 structure, none of the structurally characterized GPCRs featured a similar disulfide bridge. Like the previous rhodopsin-based models, our current models incorporate all the experimentally derived structural features mentioned above, including the aforementioned pair of extracellular disulfide bridges and the salt bridge connecting EL2 with the extracellular end of TM6. These features, contribute to shaping of the opening of the interhelical cavity lined by residues located in the extracellular N-terminus, the three extracellular loops, and all of the TMs (Figure 5).

We used the new CXCR4-based in silico structures of the $P2Y_2$ and $P2Y_4$ receptors to construct models of the putative complexes of the two receptors with compounds **11** and **16**. Importantly, we incorporated in the binding mode and in the conformation of the two ligands all the experimentally supported features shown in our previous models.[8,10,20] Moreover, we incorporated novel experimental information that we gathered through NMR spectroscopy and X-ray crystallography. Specifically, the tautomeric form of the imino group and its conformation were determined through NMR spectroscopy (chemical shift of NH at 3 position of **39** and Nuclear Overhauser Effect between MeO and the NH). Additionally, an x-ray crystallographic structure was obtained for N^4-*t*-BuO-cytosine (Supporting Information), which is in close agreement with a literature report for N^4- MeO-cytosine.[27] The data clearly showed the presence of a hydrogen atom at the 3 position and the absence of an hydrogen atom at the N^4 position. Bond lengths also indicate that that the compound adopts an exo-double bond tautomeric form.

Interestingly, the new models show several distinctive features that make them compatible with the selectivity profile compounds **11** and **16** for the $P2Y_2$ and $P2Y_4$ receptors. Specifically, the binding of nucleotides appears shifted toward the extracellular side in the new CXCR4-based models compared to those previously reported (Figure 6).[8,10,20] This is due to the fact that in the new models the side chain of $Phe^{3.32}$ (113 for $P2Y_2$, 115 for $P2Y_4$) – a residue common to all P2Y receptors and conserved as an aromatic residue ($Tyr116^{3.32}$) in the CXCR4 receptor – is parallel to the plane of the membrane. Due to this orientation, which is consistent with the one shown by $Tyr116^{3.32}$ in the crystal structure of the CXCR4 receptor, $Phe^{3.32}$ limits the depth of the binding cavity and prevents the ligands from docking at a position more distal to the extracellular side. Our previous models, which were built prior to the availability of a template containing an aromatic residue at position 3.32, featured the side chain of Phe3.32 oriented perpendicularly to the plane of the membrane and in π-stacking with the nucleobase of the ligands and allowed for a deeper binding pocket.[8,10,20] Because of the shallower binding mode proposed here in comparison to our previous rhodopsin-based models, the CXCR4-based models are compatible with the influence of the substituent at position 4 of the pyrimidine ring on the selectivity of newly synthesized compounds for $P2Y_2$ and $P2Y_4$ receptors (Figure 5). In particular, the phenyl moiety of the N^4 substituent of compound **16** protrudes toward EL2, fitting into a cavity lined by two EL2 residues, namely Thr182 and Leu184 in the $P2Y_4$ receptor. These two residues are not conserved in the $P2Y_2$ receptor, where their place is taken by Arg180 and Thr182, respectively. Our models suggest that these differences may account for the $P2Y_4$ receptor-selectivity of **16**, especially in light of the fact that the sterically bulky Arg180, conserved in the CXCR4 receptor and oriented as in the CXCR4 crystal structure, seems to

considerably reduce the volume of the cavity of the $P2Y_2$ receptor. As evident from Figure 5, this is the only region of the interhelical cavity that shows a significantly smaller volume in the $P2Y_2$ than in the $P2Y_4$ receptor.

Stability of Nucleotide Derivatives

Chemical and enzymatic instability of nucleotide analogues in biological systems is a major limitation in their use as pharmacological probes. Therefore, selected nucleotide derivatives were evaluated for stability during prolonged exposure to two different conditions. The derivatives were incubated at 37°C in aqueous medium at either low pH or in the presence of membranes prepared from 1321N1 human astrocytoma cells,[15] which contain ectonucleotidases and are representative of cells of the mammalian central nervous system. At regular intervals aliquots were taken for HPLC analysis (Figure 7).

All the nucleotide analogues tested were more stable in the presence of cell membranes than the native agonist **1**, and the most stable in the group was the Up_4-δ-phenyl ester **7**. The 4-chlorophenyl analogue **20** appeared to be more stable than the corresponding 4-methoxy **22** and 4-nitro **24** analogues. Among the nucleotide analogues tested, only Up_4-[1]glucose **8** was less stable at pH 1.5 than **1**. In general, the Up_4-δ-phenyl esters displayed a relatively high degree of stability under both conditions in comparison to **1**. Stability at pH 1.5 was also determined for the potent $P2Y_4$ receptor agonists **15, 16**, and **34**. The 5′-triphosphate derivatives **15** and **16** were similar in stability to **1**, and **34** was much more labile, similar to the closely related δ-glucose phosphoester **8** (Supporting Information).

Discussion

Pharmacological resolution of responses mediated by $P2Y_2$ versus $P2Y_4$ receptors has been problematic due to lack of selective antagonists and the fact that many analogues of **1** and diuridine tetraphosphates activate both subtypes. Two classical, general antagonists for P2 receptors, suramin and Reactive Blue 2, have been used as slightly selective antagonists of the $P2Y_2$ and $P2Y_4$ receptors, respectively.[4,31,32] In the rat, inosine-5′-triphosphate was shown to be 13-fold selective as an agonist at the $P2Y_4$ receptor in comparison to the $P2Y_2$ receptor.[32] The work described here identifies modifications that provide important new directions for introduction of agonist selectivity for $P2Y_4$ receptor ligands.

The $P2Y_4$ receptor is often expressed in the same tissues, or in some cases the same cells, as the widely distributed $P2Y_2$ receptor. This is the case for epithelial cells of the intestine. The study of knockout mice has revealed that the stimulatory effect of **1** on chloride secretion is mediated by the $P2Y_4$ receptor,[33,34] whereas its inhibitory effect on sodium absorption involves the $P2Y_2$ receptor.[35] Protective effects of $P2Y_4$ receptor activation were observed during cardiac ischemia studied in murine HL-1 myocytes.[36] $P2Y_4$ mRNA is expressed in microvascular endothelial cells isolated from mouse heart but not lung.[37] The effects of **1** on migration, proliferation, and VCAM-1 expression in these cells were greatly reduced in $P2Y_4$ receptor-deficient mice.[37] Macrophage adhesion induced by **1** also was reduced, and $P2Y_4$ receptor-null mice displayed defective angiogenesis in in-vivo models.[37] In contrast, $P2Y_2$ receptor-deficient mice exhibit reduced effects of **1** on leukocyte adhesion, eosinophil migration, and VCAM-1 expression.[38] Thus, selective $P2Y_4$ receptor agonists might prove useful in the treatment of constipation, cardiac ischemia or inflammation, and exhibit reduced proinflammatory effects in the lung due to lack of interaction with the $P2Y_2$ receptor.

Substitutions at the 4 position of the nucleobase were explored through the synthesis of imino derivatives of various sizes. The exploration of this region, done through a classic medicinal chemistry approach, was prompted by the observation, based on published models

of the $P2Y_2$ and $P2Y_4$ receptors,[8,10,20] that there might have been some space available for the expansion of the ligands around that position. This process led to the synthesis of the first $P2Y_4$-selective compounds. In particular, while N^4-(methyl)-CTP (**11**) was unselective for the two subtypes, N^4-(phenylpropoxy)-CTP (**16**), and N^4-(phenylethoxy)-CTP (**15**) were selective for the $P2Y_4$ receptor with EC_{50} values of 23 and 73 nM, respectively. The activity of these CTP analogues contrasts with the weak interaction of CTP itself at the $P2Y_2$ and $P2Y_4$ receptors.[8] Because our rhodopsin-based models could not explain the different selectivity profiles of the alkoxyimino derivatives, we reconstructed molecular models of the $P2Y_2$ and $P2Y_4$ receptors based on the recently disclosed structure of the CXCR4 receptor (Figure 5).[16] The new models incorporate all the experimentally supported features of the old ones but show a binding mode in which the ligands are slightly shifted towards the extracellular side (Figure 6), which makes them compatible with the new data. In particular, the large substituent of compounds **16** protrudes toward EL2, fitting into a cavity substantially larger in the $P2Y_4$ receptor than in the $P2Y_2$ receptor, due to the non-conservation of two specific residues. This hypothesis is in good agreement with the selectivity for the $P2Y_4$ receptor shown by compound **16**.

Moreover, by carefully probing substitution of Up_4-[1]glucose, we identified Up_4-[1]3′-deoxy-3′-fluoroglucose (**34**) as modestly $P2Y_4$ selective (EC_{50} value 62 nM). However, neither δ-phenyl esters nor methylenephosphonates were useful for achieving selectivity for the $P2Y_4$ receptor. Up_4-δ-3-chlorophenyl ester **21** was inactive at $P2Y_4$ receptors and displayed an EC_{50} value at the $P2Y_2$ receptor of 0.84 μM. The chemical and enzymatic stability of selected derivatives in this series was examined by HPLC to indicate greatly enhanced stability of the δ-phenyl phosphoesters but not the δ-glucose phosphoesters in comparison to **1**. Thus, additional SAR studies will be needed to enhance the stability of $P2Y_4$-receptor selective agonists. In particular, these studies suggest that the potency, selectivity, and stability of extended uridine tetraphosphate derivatives may be modulated by distal structural changes. N^4-Alkoxyimino analogues were analyzed in a molecular model, which indicated greater steric tolerance of the N^4-phenylpropoxy group in the $P2Y_4$ receptor.

In conclusion, we have synthesized novel uracil nucleotide derivatives that are directed toward selective activation of the $P2Y_4$ receptor. A series of homologous alkoxyimino derivatives provided an entry to novel selectivity at this subtype. Several of these compounds should be suitable for use as pharmacological probes of the physiological roles of the $P2Y_4$ receptor.

Experimental Section

Chemical Synthesis

^1H NMR spectra were obtained with a Varian Gemini 300 or Varian Mercury 400 spectrometers using D_2O, $CDCl_3$ or DMSO-d_6 as a solvent. The chemical shifts are expressed as relative ppm from HOD (4.80 ppm). ^{31}P NMR spectra were recorded at rt by use of Varian XL 300 (121.42 MHz) or Varian Mercury 400 (162.10 MHz) spectrometers; orthophosphoric acid (85%) was used as an external standard. In several cases the signal of the terminal phosphate moiety was not visible due to high dilution.

The purity of final nucleotide derivatives was checked using a Hewlett–Packard 1100 HPLC equipped with a Zorbax SB-Aq 5 μm analytical column (50 × 4.6 mm; Agilent Technologies Inc, Palo Alto, CA). Mobile phase: linear gradient solvent system: 5 mM TBAP (tetrabutylammonium dihydrogenphosphate)-CH_3CN from 80:20 to 40:60 in 13 min; the flow rate was 0.5 mL/min. Peaks were detected by UV absorption with a diode array

detector at 254, 275, and 280 nm. All derivatives tested for biological activity showed >97% purity by HPLC analysis (detection at 254 nm).

High-resolution mass measurements were performed on Micromass/Waters LCT Premier Electrospray Time of Flight (TOF) mass spectrometer coupled with a Waters HPLC system, unless noted. Purification of the nucleotide analogues for biological testing was carried out on (diethylamino)ethyl (DEAE)-A25 Sephadex columns with a linear gradient (0.01–0.5 M) of 0.5 M ammonium bicarbonate as the mobile phase. Compounds **10** was purified by Sephadex alone (and isolated in the ammonium salt form), and compounds **11** – **16** were additionally purified by HPLC with a Luna 5 μ RP-C18(2) semipreparative column (250 × 10.0 mm; Phenomenex, Torrance, CA) and using the following conditions: flow rate of 2 mL/min; 10 mM triethylammonium acetate (TEAA)-CH_3CN from 100:0 to 95:5 (System A) (or up to 99:1 to 50:50 (System B)) in 30 min (and isolated in the triethylammonium salt form). All other compounds were purified only by HPLC. All other reagents were of analytical grade, and were purchased from Sigma-Aldrich (St. Louis, MO).

Uridine-5′-β,γ-dichloromethylene triphosphate ammonium salt (10)—Uridine monophosphate sodium salt (300 mg, 0.93 mmol) and the dichloromethylenediphosphonic acid disodium salt (1 g, 3.46 mmol) were converted to the tributylammonium salts by treatment with ion-exchange resin (DOWEX 50WX2-200 (H)) and tri-*n*-butylamine. After removal of the water, the obtained tributylammonium salts were dried under high vacuum for 1 h. DIC (76.20 μL, 0.90 mmol) was added to a solution of uridine monophosphate tributylammonium salt (0.93 mmol) in DMF (3 mL). After stirring the reaction mixture at rt for 3 h, a solution of dichloromethylenediphosphonic acid tributylammonium salt (3.46 mmol) and $MgCl_2$ (171.4 mg, 1.8 mmol) in DMF (2 mL) was added. The reaction mixture was stirred at rt overnight. After removal of the solvent, the $MgCl_2$ was removed by treatment with ion-exchange resin (DOWEX 50WX2-200 (H)) and ammonia bicarbonate, and the product **10** was purified by ion-exchange column chromatography with a Sephadex-DEAE A-25 resin. ^{1}H NMR (D_2O) δ 7.96 (d, J = 7.8 Hz, 1H), 5.96 (m, 2H), 4.43 (m, 1H), 4.37 (m, 1H), 4.36 (m, 2H); ^{31}P NMR (D_2O) δ −7.77 (d, J = 18.3 Hz), −10.54 (s), −10.79 (s); HRMS-EI found 548.9043 $(M\text{-}H)^+$. $C_{10}H_{14}Cl_2N_2O_{14}P_3$ requires 548.9035; HPLC RT 9.7 min (99%) in solvent system A, 1.1 min (98%) in system B.

General procedure for the preparation of nucleoside triphosphates (11–16)

A solution of the nucleoside **39**–**44**[15] (0.073 mmol) and Proton Sponge (24 mg, 0.11 mmol) in trimethyl phosphate (0.4 mL) was stirred for 10 min at 0 °C. Then, phosphorous oxychloride (0.013 mL, 0.13 mmol) was added dropwise, and the reaction mixture was stirred for 2 h at 0 °C. A solution of tributylammonium pyrophosphate (0.8 mL, 0.44 mmol) and tri-*n*-butylamine (0.069 mL, 0.29 mmol) in *N*,*N*-dimethylformamide (DMF, 1 mL) was added and stirring was continued at 0°C for additional 10 min. 0.2 M Triethylammonium bicarbonate solution (1.5 mL) was added, and the clear solution was stirred at rt for 1 h. After removal of solvents, the residue was purified by Sephadex-DEAE A-25 resin and preparative HPLC.

***N*^{4}-Methoxycytidine-5′-triphosphate triethylammonium salt (11)—**Compound **11** (37.6 mg, 100%) was obtained as a white solid using *N*^{4}-methoxycytidine **39** (20 mg, 0.073 mmol). ^{1}H NMR (D_2O) δ 7.26 (d, *J* = 8.2 Hz, 1H), 5.96 (d, *J* = 6.4 Hz, 1H), 5.82 (d, *J* = 8.2 Hz, 1H), 4.46-4.41 (m, 1H), 4.41-4.37 (m, 1H), 4.28-4.15 (m, 3H), 3.80 (s, 3H); ^{31}P NMR (D_2O) δ −11.39 (br), −22.90 (br); HRMS-EI found 511.9873 $(M - H^+)^-$. $C_{10}H_{17}N_3O_{15}P_3$ requires 511.9857; purity > 98% by HPLC (System B: 9.08 min).

***N*^{4}-Ethoxycytidine-5′-triphosphate triethylammonium salt (12)—**Compound **12** (21.3 mg, 58%) was obtained as a white solid using N^4-ethoxycytidine **40** (20 mg, 0.070 mmol). ^{1}H NMR (D_2O) δ 7.26 (d, *J* = 7.8 Hz, 1H), 5.96 (d, *J* = 6.6 Hz, 1H), 5.82 (d, *J* = 7.8 Hz, 1H), 4.47-4.42 (m, 1H), 4.41-4.34 (m, 1H), 4.28-4.22 (m, 2H), 4.21-4.13 (m, 1H), 4.05 (dd, *J* = 14.2, 7.1 Hz, 2H); ^{31}P NMR (D_2O) δ - 11.29 (br), −22.10 (br); HRMS-EI found 526.0029 $(M - H^+)^-$. $C_{11}H_{19}N_3O_{15}P_3$ requires 526.0029; purity > 98% by HPLC (System B: 10.6 min).

***N*^{4}-*t*-Butyloxycytidine-5′-triphosphate triethylammonium salt (13)—**Compound **13** (7.6 mg, 22%) was obtained as a white solid using N^4-*t*-butoxycytidine **41** (20 mg, 0.063 mmol). ^{1}H NMR (D_2O) δ 7.24 (d, *J* = 8.2 Hz, 1H), 5.97 (d, *J* = 6.4 Hz, 1H), 5.87 (d, *J* = 8.2 Hz, 1H), 4.43-4.35 (m, 2H), 4.26-4.12 (m, 3H), 1.31 (s, 9H); ^{31}P NMR (D_2O) δ −9.85 (br), −11.36 (br), −22.99 (br); HRMS-EI found 554.0342 $(M - H^+)^-$. $C_{13}H_{23}N_3O_{15}P_3$ requires 554.0341; purity > 98% by HPLC (System B: 9.59 min).

***N*^{4}-Benzyloxycytidine-5′-triphosphate triethylammonium salt (14)—**Compound **14** (16.7 mg, 49%) was obtained as a white solid using N^4-benzyloxycytidine **42** (20 mg, 0.057 mmol). ^{1}H NMR (D_2O) δ 7.46-7.35 (m, 5H), 7.22 (d, *J* = 8.4 Hz, 1H), 5.95 (d, *J* = 6.5 Hz, 1H), 5.76 (d, *J* = 8.4 Hz, 1H), 5.05 (s, 2H), 4.43-4.32 (m, 2H), 4.26-4.13 (m, 3H); ^{31}P NMR (D_2O) δ −10.18 (br), −11.56 (d, *J* = 14.6 Hz), −23.21(t, *J* = 15.0 Hz); HRMS-EI found 588.0186 $(M - H^+)^-$. $C_{16}H_{21}N_3O_{15}P_3$ requires 588.0200; purity > 98% by HPLC (System B: 10.14 min).

***N*^{4}-Phenylethoxycytidine-5′-triphosphate triethylammonium salt (15)—**Compound **15** (1.29 mg, 5.5%) was obtained as a white solid using N^4-(2-phenylethoxy)-cytidine **43** (10 mg, 0.027 mmol). ^{1}H NMR (D_2O) δ 7.40-7.29 (m, 5H), 7.23 (d, *J* = 7.6 Hz, 1H), 5.94 (d, *J* = 6.0 Hz, 1H), 5.81 (d, *J* = 8.4 Hz, 1H), 4.43-4.38 (m, 2H), 4.28-4.25 (m, 5H), 3.00 (dd, *J* = 6 Hz, *J* = 6.4 Hz); HRMS-EI found 602.0342 $(M - H^+)^-$. $C_{17}H_{23}N_3O_{15}P_3$ requires 602.0318; purity > 98% by HPLC.

***N*^{4}-Phenylpropoxycytidine-5′-triphosphate triethylammonium salt (16)—**Compound **16** (0.83 mg, 11%) was obtained as a white solid using N^4-(3-phenylpropoxy)-cytidine **44** (5 mg, 0.013 mmol). ^{1}H NMR (D_2O) δ 7.38-7.31 (m, 5H), 7.23 (d, *J* = 8.4 Hz, 1H), 5.95 (d, *J* = 6.0 Hz, 1H), 5.78 (d, *J* = 8.4 Hz, 1H), 4.42-4.38 (m, 2H), 4.25-4.23 (m, 3H), 4.06 (dd, *J* = 5.5 Hz, *J* = 6.1 Hz, 2H), 2.75 (dd, *J* = 7.28 Hz, *J* = 7.45 Hz, 2H), 4.20 (m, 2H); ^{31}P NMR (D_2O) δ −5.51 (m), −10.34 (m), −10.81 (m); HRMS-EI found 616.0486 $(M - H^+)^-$. $C_{18}H_{25}N_3O_{15}P_3$ requires 616.0496; purity > 98% by HPLC.

General procedure for the preparation of nucleoside tetraphosphate phenyl derivatives (20–25)

The corresponding aryl monophosphate[15] (0.036 mmol) and **1** as a trisodium salt (10 mg, 0.018 mmol) were converted to the tributylammonium salts by treatment with ion-exchange resin (DOWEX 50WX2-200 (H)) and tri-*n*-butylamine. After removal of the water, the obtained tributylammonium salts were dried under high vacuum for 1 h. DIC (3.05 μL, 0.036 mmol) was added to a solution of uridine triphosphate tributylammonium salt (0.018 mmol) in DMF (0.2 mL). After stirring the reaction mixture at rt for 1 h, a solution of the corresponding aryl monophosphate tributylammonium salt (0.036 mmol) and $MgCl_2$ (3.43 mg, 0.036 mmol) in DMF (0.1 mL) was added. The reaction mixture was stirred at rt overnight. After removal of the solvent, the $MgCl_2$ was removed by treatment with ion-exchange resin (DOWEX 50WX2-200 (H)) and ammonia bicarbonate or tri-*n*-butylamine, and the residue was purified by a semipreparative HPLC.

Uridine-5′-(4-chlorophenyl)-tetraphosphate triethylammonium salt (20)— Compound **20** (0.3 mg, 6%) was obtained as a white solid using **1** (12 mg, 0.022 mmol). ^{1}H NMR (D_2O) δ 7.93 (d, *J* = 7.5 Hz, 1H), 7.38 (d, *J* = 8.4 Hz, 2H), 7.25 (d, *J* = 8.4 Hz, 2H), 5.97 (d, *J* = 5.4 Hz, 1H), 5.93 (d, *J* = 7.8 Hz, 1H), 4.42-4.30 (m, 2H), 4.27-4.21 (m, 3H); ^{31}P NMR (D_2O) δ −11.20 (br), −15.74 (br), −23.04 (br); HRMS-EI found 672.9218 $(M - H^+)^-$. $C_{15}H_{18}N_2O_{18}P_4Cl$ requires 672.9194; purity > 98% by HPLC (System B: 11.9 min).

Uridine-5′-(3-chlorophenyl)- tetraphosphate triethylammonium salt (21)— Compound **21** (1.4 mg, 12%) was obtained as a white solid using **1** (10 mg, 0.018 mmol). ^{1}H NMR (D_2O) δ 7.88 (d, *J* = 8.1 Hz, 1H), 7.36-7.12 (m, 4H), 5.91 (d, *J* = 5.1 Hz, 1H), 5.79 (d, *J* = 8.1 Hz, 1H), 4.39-4.28 (m, 2H), 4.23-4.17 (m, 3H); ^{31}P NMR (D_2O) δ −11.20 (d, *J* = 18.3 Hz), −15.84 (d, *J* = 17.5 Hz), −23.14 (m); HRMS-EI found 672.9218 $(M - H^+)^-$. $C_{15}H_{18}N_2O_{18}P_4Cl$ requires 672.9194; purity > 98% by HPLC (System B: 12.2 min).

Uridine-5′-(4-methoxyphenyl)- tetraphosphate triethylammonium salt (22)— Compound **22** (2.7 mg, 22%) was obtained as a white solid using **1** (10 mg, 0.018 mmol). ^{1}H NMR (D_2O) δ 7.88 (d, *J* = 8.4 Hz, 1H), 7.17 (d, *J* = 9.0 Hz, 2H), 6.92 (d, *J* = 9.0 Hz, 2H), 5.91 (d, *J* = 5.1 Hz, 1H), 5.88 (d, *J* = 8.4 Hz, 1H), 4.37-4.25 (m, 2H), 4.23-4.16 (m, 3H), 3.78 (s, 3H); ^{31}P NMR (D_2O) δ −11.19 (br, 1H), −15.04 (br, 1H), −23.00 (br, 2H); HRMS-EI found 668.9681 $(M - H^+)^-$. $C_{16}H_{21}N_2O_{19}P_4$ requires 668.9689; purity > 98% by HPLC (System A: 12.1 min).

Uridine-5′-(3-methoxyphenyl)- tetraphosphate triethylammonium salt (23)— Compound **23** (1.9 mg, 16%) was obtained as a white solid using **1** (10 mg, 0.018 mmol). ^{1}H NMR (D_2O) δ 7.89 (d, *J* = 8.1 Hz, 1H), 7.26 (t, *J* = 8.1 Hz, 1H), 6.90-6.82 (m, 2H), 6.72 (d, *J* = 8.1 Hz, 1H), 5.91 (d, *J* = 6.0 Hz, 1H), 5.88 (d, *J* = 8.7 Hz, 1H), 4.38-4.24 (m, 2H), 4.22-4.16 (m, 3H), 3.80 (s, 3H); ^{31}P NMR (D_2O) δ −11.20 (d, *J* = 18.4 Hz, 1H), −15.69 (d, *J* = 17.5 Hz, 1H), −23.14 (m, 2H); HRMS-EI found 668.9699 $(M - H^+)^-$. $C_{16}H_{21}N_2O_{19}P_4$ requires 668.9689; purity > 98% by HPLC (System A: 12.1 min).

Uridine-5′-(4-nitrophenyl)- tetraphosphate triethylammonium salt (24)— Compound **24** (2.2 mg, 23%) was obtained as a white solid using **1** (12 mg, 0.022 mmol). ^{1}H NMR (D_2O) δ 8.23 (d, *J* = 8.7 Hz, 2H), 7.87 (d, *J* = 8.4 Hz, 1H), 7.41 (d, *J* = 8.7 Hz, 2H), 5.91 (d, *J* = 5.1 Hz, 1H), 5.87 (d, *J* = 8.4 Hz, 1H), 4.37-4.28 (m, 2H), 4.22- 4.17 (m, 3H); ^{31}P NMR (D_2O) δ-11.14 (d, *J* = 17.5 Hz, 1H), −16.83 (d, *J* = 16.9 Hz, 1H), −23.06 (m, 2H); HRMS-EI found 683.9434 $(M - H^+)^-$. $C_{15}H_{18}N_3O_{20}P_4$ requires 683.9434; purity > 98% by HPLC (System A: 11.6 min).

Uridine-5′-(3-nitrophenyl)- tetraphosphate triethylammonium salt (25)— Compound **25** (3.4 mg, 41%) was obtained as a white solid using **1** (10 mg, 0.018 mmol). ^{1}H NMR (D_2O) δ 8.27 (d, *J* = 12.0 Hz, 2H), 7.92 (d, *J* = 8.1 Hz, 1H), 7.44 (d, *J* = 12.0 Hz, 2H), 5.96-5.88 (m, 2H), 4.41-4.30 (m, 2H), 4.25-4.19 (m, 3H); ^{31}P NMR (D_2O) δ-11.18 (d, *J* = 14.5 Hz), −16.89 (d, *J* = 14.5 Hz), −22.80 − 23.60 (m); HRMS-EI found 683.9434 $(M - H)^-$. $C_{15}H_{18}N_3O_{20}P_4$ requires 683.9438; purity > 98% by HPLC (System A: 13.1 min).

Uridine-5′-glucose-1′-β,γ-dichloromethylene tetraphosphate triethylammonium salt (26)—Compound **10** (3.4 mg, 0.006 mmol) and glucose-1-phosphate disodium salt hydrate (4 mg, 0.036 mmol) were converted to the tributylammonium salts by treatment with ion-exchange resin (DOWEX 50WX2-200 (H)) and tri-*n*-butylamine. After removal of the water, the obtained tributylammonium salts were

dried under high vacuum for 1 h. DIC (3.05 μL, 0.036 mmol) was added to a solution of **10** (0.006 mmol) in DMF (0.2 mL). After stirring the reaction mixture at rt for 1 h, a solution of glucose-1-phosphate tributylammonium salt (0.036 mmol) and $MgCl_2$ (3.43 mg, 0.036 mmol) in DMF (0.1 mL) was added. The reaction mixture was stirred at rt overnight. After removal of the solvent, the $MgCl_2$ was removed by treatment with ion-exchange resin (DOWEX 50WX2-200 (H)) and ammonia bicarbonate or tri-*n*-butylamine, and the residue was purified by a semipreparative HPLC to obtain **26** (0.32 mg, 7%) as a white solid. ^{1}H NMR (D_2O) δ 8.02 (d, J = 8.1 Hz, 1H), 6.04-5.97 (m, 2H), 5.71-5.67 (m, 1H), 4.53-4.47 (m, 1H), 4.44-4.38 (m, 1H), 4.37-4.25 (m, 3H), 4.00-3.73 (m, 4H), 3.57-3.41 (m, 2H); ^{31}P NMR (D_2O) δ 8.08 (d, J = 19.1 Hz), 1.90-0.02 (br), −10.48 (s), −10.74 (s); HRMS-EI found 790.9233 $(M\text{-}H^+)^-$. $C_{16}H_{26}N_2O_{22}P_4Cl$ requires 790.9227; purity > 98% by HPLC (System A: 10.3 min).

General procedure for the preparation of nucleoside tetraphosphate sugars (28–37)

The appropriate sugar **63** – **67** was treated with a mixture of sodium acetate (50 mg) in acetic anhydride (5 mL), and the mixture was stirred for 5 h at 110°C while following the course of the reaction by TLC. Excess Ac_2O was removed using a rotary evaporator, and the mixture was stirred with aq. $NaHCO_3$ for 15 min. The product was extracted into dichloromethane and washed with brine. The corresponding crude acetyl derivative was purified by column chromatography. The monophosphate derivatives (**68**– **72**) of these acetyl sugars were prepared as the lithium salts using the MacDonald procedure.[39] The corresponding sugar monophosphate (0.036 mmol) and uridine triphosphate trisodium salt (10 mg, 0.018 mmol) were converted to the tributylammonium salts by treatment with ion-exchange resin (DOWEX 50WX2-200 (H)) and tri-*n*-butylamine. After removal of the water, the obtained tributylammonium salts were dried under high vacuum for 1 h. DIC (3.05 μL, 0.036 mmol) was added to a solution of **1** as a tributylammonium salt (0.018 mmol) in DMF (0.2 mL). After stirring the reaction mixture at rt for 3 h, a solution of the corresponding sugar monophosphate tributylammonium salt (0.036 mmol), and $MgCl_2$ (3.43 mg, 0.036 mmol) in DMF (0.1 mL) was added. The reaction mixture was stirred at rt for 2 h to overnight. After removal of the solvent, the $MgCl_2$ was removed by treatment with ion-exchange resin (DOWEX 50WX2-200 (H)) and ammonia bicarbonate or tri-*n*-butylamine, and the residue was purified by a semipreparative HPLC purification using system C.

Uridine-5′-allose-1′-tetraphosphate triethylammonium salt (28)—Compound **28** (1 mg, 8%) was obtained as a white solid using **1** (10 mg, 0.018 mmol) and D-allose-1-phosphate (**69**, 16.5 mg, 0.036 mmol). ^{1}H NMR (D_2O) δ 7.95 (d, J = 8.1 Hz, 1H), 5.98 (m, 2H), 5.60 (m, 1H), 4.16 (m, 2H), 4.33 (m, 1H), 4.28-4.23 (m, 2H), 3.90-3.60 (m, 4H), 3.54 (m, 1H), 3.41 (m, 1H); ^{31}P NMR (D_2O) δ −11.29 (m), −12.40 (m), −22.86 (m); HRMS-EI found 724.9831 $(M\text{-}H)^+$. $C_{15}H_{25}N_2O_{23}P_4$ requires 724.9804; HPLC (purity 97%, System A: 11.5 min; purity 98%, System B: 0.8 min).

Uridine-5′-mannose-1′-tetraphosphate triethylammonium salt (29)—Compound **29** (3.18 mg, 24%) was obtained as a white solid using **1** (10 mg, 0.018 mmol) and D-mannose-1-phosphate (**68**, 16.5 mg, 0.036 mmol). ^{1}H NMR (D_2O) δ 7.99 (d, J = 8.4 Hz, 1H), 6.02 (m, 2H), 5.56 (m, 1H), 4.44 (m, 2H), 4.31-4.27 (m, 3H), 4.16 (m, 1H), 4.03-3.87 (m, 3H), 3.79 (m, 1H), 3.67 (m, 1H); ^{31}P NMR (D_2O) δ −11.17 (d, J = 17.6 Hz), −12.63 (d, J = 17.5 Hz), −23.10 (m); HRMS-EI found 724.9796 $(M\text{-}H)^+$. $C_{15}H_{25}N_2O_{23}P_4$ requires 724.9799; HPLC (purity 99%, System A: 10.4 min; purity 99%, System B: 1.1 min).

Uridine-5′-xylose-1′-tetraphosphate triethylammonium salt (30)—Compound **30** (3.18 mg, 43%) was obtained as a white solid using **1** (6.3 mg, 0.011 mmol) and D-xylose-1-phosphate (14 mg, 0.032 mmol). ^{1}H NMR (D_2O) δ 8.00 (d, J = 8.4 Hz, 1H), 6.07-5.98 (m,

2H), 5.64-5.58 (m, 1H), 4.50-4.40 (m, 2H), 4.36-4.23 (m, 3H), 3.83-3.76 (m, 1H), 3.69-3.60 (m, 1H), 3.58-3.49 (m, 1H), 3.47-3.37 (m, 1H); ^{31}P NMR (D_2O) δ −11.22 (d, J = 16.8 Hz), −12.65 (d, J = 18.2 Hz), −22.6 – −23.4 (m); HRMS-EI found 694.9693 $(M-H)^-$. $C_{14}H_{23}N_2O_{22}P_4$ requires 694.9656; purity > 98% by HPLC (System B: 12.3 min).

General procedure for the preparation of nucleoside tetraphosphate sugars (31 and 32)

The corresponding sodium salt of sugar monophosphate (0.036 mmol) and the trisodium salt of **1** (10 mg, 0.018 mmol) were converted to the tributylammonium salts by treatment with ion-exchange resin (DOWEX 50WX2-200 (H)) and tri-*n*-butylamine. After removal of the water, the obtained tributylammonium salts were dried under high vacuum 1 h. DIC (3.05 μL, 0.036 mmol) was added to a solution of **1** as a tributylammonium salt (0.018 mmol) in DMF (0.2 mL). After stirring the reaction mixture at rt for 3 h, a solution of the corresponding sugar monophosphate tributylammonium salt (0.036 mmol) and $MgCl_2$ (3.43 mg, 0.036 mmol) in DMF (0.1 mL) was added. The reaction mixture was stirred at rt for 2 h to overnight. After removal of the solvent, the $MgCl_2$ was removed by treatment with ion-exchange resin (DOWEX 50WX2-200 (H)) and ammonia bicarbonate or tri-*n*-butylamine, and the residue was purified by a semipreparative HPLC purification using system C.

P^1-(Uridine-5′-)P^4-(2′-deoxy-2′-acetamidoglucose-1′-)tetraphosphate triethylammonium salt (31)—Compound **31** (5.21 mg, 38%) was obtained as a white solid using **1** (10 mg, 0.018 mmol) and D-2-deoxy-2-acetamidoglucose-1-phosphate (12.5 mg, 0.036 mmol). ^{1}H NMR (D_2O) δ 7.99 (d, J = 8.1 Hz, 1H), 6.02 (m, 2H), 5.53 (m, 1H), 4.44 (m, 2H), 4.29 (m, 3H), 4.02-3.80 (m, 4H), 3.53 (m, 1H), 2.11 (s, 3H), 1.93 (s, 1H); ^{31}P NMR (D_2O) δ −11.17 (d, J = 18.3 Hz), −12.77 (d, J = 19.0 Hz), −23.10 (m); HRMS-EI found 766.0037 $(M-H)^+$. $C_{17}H_{28}N_3O_{23}P_4$ requires 766.0064; HPLC (purity 99%, System A: 10.4 min; purity 99%, System B: 0.8 min).

P^1-(Uridine-5′-)P^4-(glucuronic acid-1′-)tetraphosphate triethylammonium salt (32)—Compound **32** (2.46 mg, 18%) was obtained as a white solid using **1** (10 mg, 0.018 mmol) and α-D-glucuronic acid 1-phosphate (**74**, 12.2 mg, 0.036 mmol). ^{1}H NMR (D_2O) δ 7.95 (d, J = 7.5 Hz, 1H), 5.99 (m, 2H), 5.65 (m, 1H), 4.39 (m, 2H), 4.27-4.23 (m, 3H), 4.10 (m, 1H), 3.80 (m, 1H), 3.51 (s, 2H); ^{31}P NMR (D_2O) δ −11.18 (d, J = 17.6 Hz), −12.55 (d, J = 16.7 Hz), −22.71 (m); HRMS-EI found 738.9575 $(M-H)^+$. $C_{175}H_{23}N_2O_{24}P_4$ requires 738.9591; HPLC (purity 97%, System A: 11.4 min; purity 99%, System B: 1.0 min).

P^1-(Uridine-5′-)P^4-(2′-deoxy-2′-fluoroglucose-1′-)tetraphosphate triethylammonium salt (33)—Compound **33** (3.28 mg, 25%) was obtained as a white solid using **1** (10 mg, 0.018 mmol) and D-2-deoxy-2-fluoroglucose-1-phosphate (**70**, 16.57 mg, 0.036 mmol). ^{1}H NMR (D_2O) δ 7.99 (d, J = 8.1 Hz, 1H), 6.01 (m, 2H), 5.82 (m, 1H), 4.44 (m, 2H), 4.28 (m, 3H), 4.12-3.71 (m, 4H), 3.52 (m, 1H); ^{31}P NMR (D_2O) δ −11.10 (d, J = 16.7 Hz), −13.10 (d, J = 17.5 Hz), −23.07 (m); HRMS-EI found 726.9753 $(M-H)^+$. $C_{15}H_{24}FN_2O_{23}P_4$ requires 726.9761; HPLC (purity 99%, System A: 10.3 min; purity 98%, System B: 1.1 min).

P^1-(Uridine-5′-)P^4-(3′-deoxy-3′-fluoroglucose-1′-)tetraphosphate triethylammonium salt (34)—Compound **34** (3.58 mg, 27%) was obtained as a white solid using **1** (10 mg, 0.018 mmol) and D-3-deoxy-3-fluoroglucose-1-phosphate (**71**, 16.57 mg, 0.036 mmol). ^{1}H NMR (D_2O) δ 7.92 (d, J = 8.1 Hz, 1H), 5.98 (m, 2H), 5.61 (m, 1H), 4.35 (m, 2H), 4.27-4.21 (m, 4H), 3.99-3.72 (m, 3H); ^{31}P NMR (D_2O) δ −11.08 (m), −12.87 (m), −22.38 (m); HRMS-EI found 726.9763 $(M-H)^+$. $C_{15}H_{24}FN_2O_{23}P_4$ requires 726.9761; HPLC (purity 98%, System A: 10.4 min; purity 98%, System B: 1.0 min).

P^1-(N^4-Benzyloxycytidine-5′-)P^4-(3′-deoxy-3′-fluoroglucose-1′-)tetraphosphate triethylammonium salt (35)—Compound **35** (0.550 mg, 2.6%) was obtained as a white solid using triethylammonium salt of N^4-benzyloxycytidine 5′-triphosphate (14.45 mg, 0.018 mmol) and D-3-deoxy-3-fluoroglucose-1-phosphate (**71**, 14.76 mg, 0.036 mmol). ^{1}H NMR (D_2O) δ 7.44 (m, 5H), 7.23 (d, J = 8.8 Hz, 1H), 5.96 (d, J = 6.4 Hz, 1H), 5.77 (d, J = 8.4 Hz, 1H), 5.05 (s, 2H), 4.46-4.42 (m, 2H), 4.38-4.17 (m, 4H), 3.99-3.72 (m, 3H); ^{31}P NMR (D_2O) δ −11.53 (m), −13.27 (m), −23.21 (m); HRMS-EI found 832.0319 $(M-H)^+$. $C_{22}H_{31}FN_3O_{22}P_4$ requires 726.9761.

P^1-(N^4-Methoxycytidine-5′-)P^4-(3′-deoxy-3′-fluoroglucose-1′-)tetraphosphate triethylammonium salt (36)—Compound **36** (0.80 mg, 8.8%) was obtained as a white solid using triethylammonium salt of N^4-methoxycytidine 5′-triphosphate (9 mg, 0.012 mmol) and D-3-deoxy-3-fluoroglucose-1-phosphate (**71**, 10 mg, 0.025 mmol). ^{1}H NMR (D_2O) δ 7.26 (d, J = 7.6 Hz, 1H), 5.96 (d, J = 6.92 Hz, 1H), 5.83 (d, J = 8.2 Hz, 1H), 5.69 (m, 1H), 4.42-4.37 (m, 2H), 4.26-4.15 (m, 4H), 3.99-3.89 (m, 2H), 3.80 (m, 5H); HRMS-EI found 756.0002 $(M-H)^+$. $C_{16}H_{27}FN_3O_{24}P_4$ requires 756.0021; purity 97% by HPLC (System B: 13.5 min).

P^1-(Uridine-5′-)P^4-(4′-deoxy-4′-fluoroglucose-1′-)tetraphosphate triethylammonium salt (37)—Compound **37** (2.88 mg, 22%) was obtained as a white solid using **1** (10 mg, 0.018 mmol) and D-4-deoxy-4-fluoroglucose-1-phosphate (**72**, 16.57 mg, 0.036 mmol). ^{1}H NMR (D_2O) δ 7.99 (d, J = 8.1 Hz, 1H), 6.02 (m, 2H), 5.66 (m, 1H), 4.45 (m, 2H), 4.28 (m, 3H), 4.17-4.06 (m, 2H), 3.99-3.77 (m, 2H), 3.60 (m, 1H); ^{31}P NMR (D_2O) δ −11.12 (d, J = 17.6 Hz), −12.70 (d, J = 16.6 Hz), −23.17 (m); HRMS-EI found 726.9753 $(M-H)^+$. $C_{15}H_{24}FN_2O_{23}P_4$ requires 726.9761; HPLC (purity 97%, System A: 11.0 min; purity 99%, System B: 1.1 min).

α-D-Glucuronic acid 1-phosphate trisodium salt (74)

TEMPO (10 mg, 64 μmol) was added to a solution of α-D-glucose-1-phosphate disodium salt (**73**, 4.13 g, 13.6 mmol) in H_2O (4 mL) at 0°C. To this solution, aqueous 1 M NaOH was added until pH 9 was reached, and a NaOCl solution (1.2 mL, available chlorine: 10–13%) was added slowly. The pH was maintained at 9 by adding 1 M NaOH aq. several times during the reaction. After 1.5 h, MeOH was added to the reaction mixture, and the resulting precipitate was collected by filtration to give **74** (415 mg, 90%) as a white solid. ^{1}H-NMR (D_2O) δ5.46 (dd, 1H, J=3.6, 7.5 Hz), 4.15 (d, 1H, J=10.2 Hz), 3.79 (t, 1H, J=9.6 Hz), 3.48 (d, 1H, J=9.6 Hz), 3.47 (t, 1H, J=9.6 Hz); HRMS-ES^- found 294.9831 $(M+Na-2H)^-$. $C_6H_9O_{10}PNa$ requires 294.9837.

Assay of PLC activity stimulated by $P2Y_2$, $P2Y_4$, and $P2Y_6$ receptors

Stable cell lines expressing the human $P2Y_2$, $P2Y_4$, or $P2Y_6$ receptor in 1321N1 human astrocytoma cells were generated as described.[19] Agonist-induced [^{3}H]inositol phosphate production was measured in in 96-well plates that received 20,000 cells/well two days prior to assay. Sixteen h before the assay, the inositol lipid pool of the cells was radiolabeled by incubation in 100 μL of serum-free inositol-free Dulbecco's modified Eagle's medium, containing 1.0 μCi of *myo*-[^{3}H]inositol. No changes of medium were made subsequent to the addition of [^{3}H]inositol. On the day of the assay, cells were challenged with 25 μL of a five-fold concentrated solution of receptor agonists in 200 mM HEPES (N-(2-hydroxyethyl)-piperazine-N′-2-ethanesulfonic acid), pH 7.3 in Hank's balanced salt solution, containing 50 mM LiCl for 30 min at 37°C. Incubations were terminated by aspiration of the drug-containing medium and addition of 450 μL of ice-cold 50 mM formic acid. [^{3}H]Inositol phosphate accumulation was quantified using scintillation proximity assay methodology as previously described in detail.[19]

Data Analysis

Agonist potencies (EC_{50} values) were determined from concentration-response curves by non-linear regression analysis using the GraphPad software package Prism (GraphPad, San Diego, CA). All experiments examining the activity of newly synthesized molecules also included full concentration effect curves for the cognate agonist of the target receptor: **1** for the $P2Y_2$ and $P2Y_4$ receptors and UDP for the $P2Y_6$ receptor. Each concentration of drug was tested in triplicate assays, and concentration effect curves for each test drug were repeated in at least three separate experiments with freshly diluted molecule. The results are presented as mean ± SEM from multiple experiments or in the case of concentration effect curves from a single experiment carried out with triplicate assays that were representative of results from multiple experiments.

Molecular Modeling

Molecular models of the $P2Y_2$ and $P2Y_4$ receptors were constructed with the Molecular Operating Environment (MOE)[40] on the basis of the crystal structure of the CXCR4 chemokine receptor.[16] An initial sequence alignment was obtained with the Blosum62 substitution matrix, with penalties for gap insertions and extensions of 7 and 1, respectively. The proper alignment of the conserved motifs that characterize each of the TM helices was checked and, when necessary, manually adjusted. All the gaps in the alignment of the TM helices were eliminated; gaps in the loops were consolidated into a single gap per loop, and positioned where insertions or deletions seemed compatible with the structure of the template. The final alignment used for the construction of the model is provided in Figure 3. Ten models were built and scored on the basis of electrostatic solvation energy (GB/VI).[41] Intermediate and final models were subjected to energy minimizations with the Amber99 force field, according to the protocol implemented in MOE, with the refinement level set to medium.[40]

As mentioned, a disulfide bridge connects the N-terminus and the extracellular end of TM7 in the CXCR4 receptor and, putatively, in the P2Y receptors, according to mutagenesis data.[22–24] However, as evident from Figure 3, in the P2Y receptors this cysteine residue is shifted two residues downstream with respect to the CXCR4 receptor. Thus, before the construction of the homology model, the N-terminal region of the template was modified *ad hoc*. In particular, Cys28 and Arg30 of CXCR4 were mutated to alanine and cysteine, respectively, and a disulfide bridge was built between Cys28 and Cys274. The mutated CXCR4 receptor was then subjected to energy minimization with MOE,[37] with the Amber99 force field, until reaching a cutoff parameter on the potential energy gradient of 0.05 kcal/(mol·Å). During the minimization, the two cysteines and all the N-terminal residues were granted flexibility.

After the construction of the homology models, **1** was docked into the $P2Y_2$ and $P2Y_4$ receptors superimposing our previously published complexes to the new models. For each receptor, the ligand was then subjected to two subsequent energy minimizations, the first holding the receptor frozen, the second one granting flexibility to all residues within a 5 Å radius from the ligand. The energy minimizations were conducted in MOE,[40] with the MMFFx force field, until reaching a cutoff parameter on the potential energy gradient of 0.05 kcal/(mol·Å). Compounds **11** and **16** were then sketched from **1** within the $P2Y_2$ and $P2Y_4$ receptors, respectively, and subsequently subjected to the same two rounds of minimization following the same protocol outlined above for **1**. The obtained $P2Y_2$-**11** and $P2Y_4$-**16** complexes were subsequently transferred to Maestro[42] and subjected to conformational searches with the MacroModel engine,[43] as implemented in the Schrodinger package. Flexibility was granted to the ligands and the residues within a 5 Å radius from them. All of the atoms within an additional shell of a 3 Å radius were also taken into account

as a frozen environment. The calculations were conducted with the MMFFs force field, using water as implicit solvent (GB/SA model).[44] The minimizations were based on the Polak-Ribiere conjugate gradient algorithm and were performed with a threshold on the potential energy gradient of 0.05 kcal/(mol·Å). The conformational searches were based on 100 steps of extended Monte Carlo Multiple Minimum (MCMM) sampling protocol. Specifically, the sampling regarded all torsion angles of residues and ligands, as well as ligand rotation and ligand translation.

The interhelical cavities of the $P2Y_2$ and $P2Y_4$ receptor were analyzed with the SiteMap program, implemented in the Schrodinger package, cropping site maps at 2 Å from the nearest site point.[44]

Stability of Nucleotide Derivatives

Compound **1** was purchased from Sigma (St. Louis, MO). Compound **2** was synthesized by the procedure previously reported.[13] HCl buffer (pH 1.5) solution was prepared as follows. Concentrated HCl (7 mL, 12 N) was added to 2.0 g of sodium chloride and diluted with water to a volume of 1000 mL. Membranes were prepared as follows. $P2Y_1$ receptor-expressing astrocytoma cells were grown to 80% confluence and then harvested. The cells were homogenized and the nuclear fraction was removed by centrifuging at 100 × g for 5 min. The pellet was resuspended in 50 mM tris(hydroxymethyl)aminomethane (Tris) hydrochloride buffer (pH 7.4). The suspension was homogenized with a polytron homogenizer (Brinkmann) for 10 s and was ultracentrifuged at 20,000 × g for 20 min at 4°C. The resultant pellets were resuspended in Tris buffer (pH 7.4), and the membrane was stored at −80° C until the experiments. The protein concentration of the membrane preparation was measured using the Bradford assay.[45] The membrane preparation was diluted with 4 mL of Dulbecco's phosphate-buffered saline (pH 7.4) and homogenized before use for the stability check. The final protein concentration was 14.9 μg/mL.

Ten μL of a 2 mg/mL aqueous solution of each nucleotide derivative was mixed with either 90 μL of HCl buffer (pH 1.2) or the membrane suspension and incubated at 37°C. At regular intervals, a 6 μL aliquot of the above mixture (either membranes or low pH) removed. The injection sample was pre-diluted with 54 μL of 5 mM tetrabutylammonium dihydrogenphosphate (TBAP) to allow complete equilibration with the mobile phase to avoid the early HPLC elution at ~1 min. Then, 50 μL of the mixture was injected to the HPLC.

AUC of compounds were measured using a Hewlett–Packard 1100 HPLC equipped with a Zorbax Eclipse 5 mm XDB-C18 analytical column (250 × 4.6 mm; Agilent Technologies Inc, Palo Alto, CA). Mobile phase: linear gradient solvent system: 5 mM TBAP-CH_3CN from 80:20 to 40:60 in 6.5 min; the flow rate was 1 mL/min (System C) or System B. Peaks were detected by UV absorption with a diode array detector at 254, 275, and 280 nm and AUC were calculated based on the peak at 254 nm.

Supplementary Material

Refer to Web version on PubMed Central for supplementary material.

Abbreviations

CTP	cytidine-5′-triphosphate
DIC	*N*,*N*′-diisopropylcarbodiimide

DMF	*N*,*N*-dimethylformamide
EL	extracellular loop
GPCR	G protein-coupled receptor
HEPES	*N*-2-hydroxyethylpiperazine-*N*′-2-ethanesulfonic acid
HPLC	high performance liquid chromatography
IL	intracellular loop
MOE	Molecular Operating Environment
SAR	structure activity relationship
TBAP	tetrabutylammonium dihydrogenphosphate
TEAA	triethylammonium acetate
TEMPO	2,2,6,6-tetramethylpiperidine-1-oxyl
TM	transmembrane α-helix
TMS	trimethylsilyl
UMP	uridine-5′-monophosphate
UDP	uridine-5′-diphosphate
UTP	uridine-5′-triphosphate

Acknowledgments

X-ray determination was performed by Dr. Yoshiaki Oyama, Asubio Pharmaceuticals, Osaka, Japan. Mass spectral measurements were performed by Dr. Noel Whittaker (NIDDK). We thank Dr. Francesca Deflorian (NIDDK) and Dr. Andrei A. Ivanov (Emory Univ.) for helpful discussions. This research was supported in part by NIGMS research grant GM38213 and by the Intramural Research Program of NIDDK, National Institutes of Health. H. Maruoka thanks Asubio Pharma Co., Ltd. for financial support. S. de Castro thanks Ministerio de Educacio´n y Ciencia (Spain) for financial support.

References

1. Abbracchio MP, Burnstock G, Boeynaems JM, Barnard EA, Boyer JL, Kennedy C, Fumagalli M, King BF, Gachet C, Jacobson KA, Weisman GA. International Union of Pharmacology LVIII: update on the P2Y G protein-coupled nucleotide receptors: from molecular mechanisms and pathophysiology to therapy. Pharmacol. Rev. 2006; 58:281–341. [PubMed: 16968944]
2. Brunschweiger A, Müller CE. P2 Receptors activated by uracil nucleotides - An update. Current Med. Chem. 2006; 13:289–312.
3. Nicholas RA, Lazarowski ER, Watt WC, Li Q, Harden TK. Uridine nucleotide selectivity of three phospholipase C-activating P2 receptors: identification of a UDP-selective, a UTP-selective, and an ATP- and UTP-specific receptor. Mol. Pharmacol. 1996; 50:224–229. [PubMed: 8700127]
4. Communi D, Motte S, Boeynaems JM, Pirotton S. Pharmacological characterization of the human $P2Y_4$ receptor. Eur. J. Pharmacol. 1996; 317:383–389. [PubMed: 8997625]
5. Shaver SR, Rideout JL, Pendergast W, Douglass JG, Brown EG, Boyer JL, Patel RI, Redick CC, Jones AC, Picher M, Yerxa BR. Structure activity relationships of dinucleotides: Potent and selective agonists of P2Y receptors. Purinergic Signalling. 2005; 1:183–191. [PubMed: 18404503]
6. Yerxa BR, Sabater JR, Davis CW, Stutts MJ, Lang-Furr M, Picher M, Jones AC, Cowlen M, Dougherty R, Boyer J, Abraham WM, Boucher RC. Pharmacology of INS37217 [P(1)-(uridine 5')-P(4)- (2'-deoxycytidine 5')tetraphosphate, tetrasodium salt], a next-generation $P2Y_2$ receptor agonist for the treatment of cystic fibrosis. J. Pharmacol. Exp. Ther. 2002; 302:871–880. [PubMed: 12183642]

7. Kellerman D, Rossi Mospan A, Engels J, Schaberg A, Gorden A, Smiley L. Denufosol: A review of studies with inhaled $P2Y_2$ agonists that led to Phase 3. Pulm. Pharmacol. Ther. 2008; 21:600–607. [PubMed: 18276176]
8. Jacobson K, Costanzi S, Ivanov A, Tchilibon S, Besada P, Gao Z, Maddileti S, Harden T. Structure activity and molecular modeling analyses of ribose- and base-modified uridine 5'-triphosphate analogues at the human $P2Y_2$ and $P2Y_4$ receptors. Biochem. Pharmacol. 2006; 71:540–549. [PubMed: 16359641]
9. Davenport RJ, Diaz P, Galvin FC, Lloyd S, Mack SR, Owens R, Sabin V, Wynn J. Novel nucleotide triphosphates as potent $P2Y_2$ agonists with enhanced stability over UTP. Bioorg. Med. Chem. Lett. 2007; 17:558–561. [PubMed: 17079144]
10. Ivanov A, Ko H, Cosyn L, Maddileti S, Besada P, Fricks I, Costanzi S, Harden T, Calenbergh S, Jacobson K. Molecular modeling of the human $P2Y_2$ receptor and design of a selective agonist, 2'-amino-2'-deoxy-2-thiouridine 5'-triphosphate. J. Med. Chem. 2007; 50:1166–1176. [PubMed: 17302398]
11. Kim HS, Ravi RG, Marquez VE, Maddileti S, Wihlborg A-K, Erlinge D, Malmsjö M, Boyer JL, Harden TK, Jacobson KA. Methanocarba modification of uracil and adenine nucleotides: High potency of Northern ring conformation at $P2Y_1$, $P2Y_2$, $P2Y_4$ and $P2Y_{11}$, but not $P2Y_6$ receptors. J. Med. Chem. 2002; 45:208–218. [PubMed: 11754592]
12. El-Tayeb A, Qi A, Müller CE. Synthesis and Structure-Activity Relationships of Uracil Nucleotide Derivatives and Analogues as Agonists at Human $P2Y_2$, $P2Y_4$, and $P2Y_6$ Receptors. J. Med. Chem. 2006; 49:7076–7087. [PubMed: 17125260]
13. Ko H, Carter RL, Cosyn L, Petrelli R, de Castro S, Besada P, Zhou Y, Cappellacci L, Franchetti P, Grifantini M, Van Calenbergh S, Harden TK, Jacobson KA. Synthesis and potency of novel uracil nucleotide analogues as $P2Y_2$ and $P2Y_6$ receptor agonists. Bioorg. Med. Chem. 2008; 16:6319–6332. [PubMed: 18514530]
14. Sauer R, El-Tayeb A, Kaulich M, Müller CE. Synthesis of uracil nucleotide analogs with a modified, acyclic ribose moiety as $P2Y_2$ receptor antagonists. Bioorg. Med. Chem. 2009; 17:5071–5079. [PubMed: 19523835]
15. Maruoka H, Barrett MO, Ko H, Tosh DK, Melman A, Burianek LE, Balasubramanian R, Berk B, Costanzi S, Harden TK, Jacobson KA. Pyrimidine Ribonucleotides with Enhanced Selectivity as $P2Y_6$ Receptor Agonists: Novel 4-Alkyloxyimino, (S)-Methanocarba, and 5'-Triphosphate γ-Ester Modifications. J. Med. Chem. 2010; 53:4488–4501. [PubMed: 20446735]
16. Wu B, Chien EY, Mol CD, Fenalti G, Liu W, Katritch V, Abagyan R, Brooun A, Wells P, Bi FC, Hamel DJ, Kuhn P, Handel TM, Cherezov V, Stevens RC. Structures of the CXCR4 chemokine GPCR with small-molecule and cyclic peptide antagonists. Science. 2010; 330:1066–1071. [PubMed: 20929726]
17. Kogo S, Yamada K, Iwai Y, Osawa K, Hayakawa H. Process for Producing Di(pyrimidine nucleoside 5'-)polyphosphate. 2008 WO2008/012949 A1.
18. Heeres A, van Doren HA, Gotlieb KF, Bleeker IP. Synthesis of α- and β- D- glucopyranuronate 1-phosphate and α-D-glucopyranuronate 1-fluoride: Intermediates in the synthesis of D-glucuronic acid from starch. Carbohydrate Res. 1997; 299:221–227.
19. Bourdon DM, Wing MR, Edwards EB, Sondek J, Harden TK. Quantification of isozyme-specific activation of phospholipase C-β 2 by Rac GTPases and phospholipase C-ε by Rho GTPases in an intact cell assay system. Methods Enzymol. 2006; 406:489–499. [PubMed: 16472681]
20. Costanzi S, Mamedova L, Gao Z, Jacobson K. Architecture of P2Y nucleotide receptors: structural comparison based on sequence analysis, mutagenesis, and homology modeling. J. Med. Chem. 2004; 47:5393–5404. [PubMed: 15481977]
21. de Castro S, Maruoka H, Hong K, Kilbey SM 2nd, Costanzi S, Hechler B, Brown GG Jr, Gachet C, Harden TK, Jacobson KA. Functionalized congeners of $P2Y_1$ receptor antagonists: 2-alkynyl (N)-methanocarba 2'-deoxyadenosine 3',5'-bisphosphate analogues and conjugation to a polyamidoamine (PAMAM) dendrimer carrier. Bioconjugate Chem. 2010; 21:1190–205.
22. Hoffmann C, Moro S, Nicholas RA, Harden TK, Jacobson KA. The role of amino acids in extracellular loops of the human $P2Y_1$ receptor in surface expression and activation processes. J. Biol. Chem. 1999; 274:14639–14647. [PubMed: 10329657]

23. Moro S, Hoffmann C, Jacobson KA. Role of the extracellular loops of G protein- coupled receptors in ligand recognition: a molecular modeling study of the human $P2Y_1$ receptor. Biochemistry. 1999; 38:3498–3507. [PubMed: 10090736]
24. Hillmann P, Ko GY, Spinrath A, Raulf A, von Kugelgen I, Wolff SC, Nicholas RA, Kostenis E, Holtje HD, Muller CE. Key determinants of nucleotide-activated G protein-coupled $P2Y_2$ receptor function revealed by chemical and pharmacological experiments, mutagenesis and homology modeling. J. Med. Chem. 2009; 52:2762–2775. [PubMed: 19419204]
25. Moro S, Guo D, Camaioni E, Boyer JL, Harden TK, Jacobson KA. Human $P2Y_1$ receptor: molecular modeling and site-directed mutagenesis as tools to identify agonist and antagonist recognition sites. J. Med. Chem. 1998; 41:1456–66. [PubMed: 9554879]
26. Jiang Q, Guo D, Lee BX, van Rhee AM, Kim YC, Nicholas RA, Schachter JB, Harden TK, Jacobson KA. A mutational analysis of residues essential for ligand recognition at the human $P2Y_1$ receptor. Mol. Pharmacol. 1997; 52:499–507. [PubMed: 9281613]
27. Van Meervelt L. Structure of 3',5'-di-*O*-acetyl-N^4-methoxycytosine. Acta Cryst. 1991; C47:2635–2637.
28. Ballesteros, JA.; Weinstein, H. Integrated methods for the construction of three-dimensional models and computational probing of structure-function relations in G protein-coupled receptors. In: Stuart, CS., editor. Methods in Neurosciences. Vol. 25. Academic Press; 1995. p. 366-428.
29. van Rhee AM, Jacobson KA. Molecular architecture of G protein-coupled receptors. Drug Develop. Res. 1996; 37:1–38.
30. Costanzi S, Tikhonova I, Ohno M, Roh E, Joshi B, Colson A, Houston D, Maddileti S, Harden T, Jacobson K. $P2Y_1$ antagonists: combining receptor-based modeling and QSAR for a quantitative prediction of the biological activity based on consensus scoring. J. Med. Chem. 2007; 50:3229–3241. [PubMed: 17564423]
31. Yitzhaki S, Shneyvais V, Jacobson KA, Shainberg A. Involvement of uracil nucleotides in protection of cardiomyocytes from hypoxic stress. Biochem. Pharmacol. 2005; 69:1215–1223. [PubMed: 15794942]
32. Wildman SS, Unwin RJ, King BF. Extended pharmacological profiles of rat $P2Y_2$ and rat $P2Y_4$ receptors and their sensitivity to extracellular H^+ and Zn^{2+} ions. Br. J. Pharmacol. 2003; 140:1177–1186. [PubMed: 14581177]
33. Robaye B, Ghanem E, Wilkin F, Fokan D, Van Driessche W, Schurmans S, Boeynaems JM, Beauwens R. Loss of nucleotide regulation of epithelial chloride transport in the jejunum of $P2Y_4$-null mice. Mol. Pharmacol. 2003; 63:777–783. [PubMed: 12644577]
34. Ghanem E, Robaye B, Leal T, Leipziger J, Van Driessche W, Beauwens R, Boeynaems JM. The role of epithelial $P2Y_2$ and $P2Y_4$ receptors in the regulation of intestinal chloride secretion. Br. J. Pharmacol. 2005; 146:364–369. [PubMed: 16056234]
35. Matos JE, Sorensen MV, Geyti CS, Robaye B, Boeynaems JM, Leipziger J. Distal colonic Na^+ absorption inhibited by luminal $P2Y_2$ receptors. Pflugers Arch. 2007; 454:977–987. [PubMed: 17356885]
36. Cosentino, S.; Barcella, S.; Lo, H.; Burbiel, JC.; Müller, CE.; Tremoli, E.; Banfi, C.; Abbracchio, MP. Purines. Tarragona, Spain: 2010. Role of P2 receptors in a cardiomyocyte ischemic hypoxia model. May 30 – June 2, 2010 Abstract P10-11
37. Horckmans M, Lantz N, Dol-Gleizes F, Savi P, Gachet C, Boeynaems JM, Robaye B, Communi D. Involvement of the $P2Y_4$ receptor in inflammation and angiogenesis. Purines 2008 Meeting 29 June – 2 July 2008, Copenhagen, Denmark. Purinergic Signal. 2008; 4 Suppl 1:118.
38. Vanderstocken G, Bondue B, Horckmans M, Di Pietrantonio L, Robaye B, Boeynaems JM, Communi D. $P2Y_2$ receptor regulates VCAM-1 membrane and soluble forms and eosinophil accumulation during lung inflammation. J. Immunol. 2010; 185:3702–3707. [PubMed: 20720203]
39. MacDonald DL. Chemical synthesis of aldose 1-phosphates. Methods Enzymol. 1966; 8:121–125. [11].
40. The molecular operating environment (MOE). Chemical Computing Group, Inc; Montreal, Canada: 2009.10, www.ccg.com

41. Labute P. The generalized Born/volume integral implicit solvent model: estimation of the free energy of hydration using London dispersion instead of atomic surface area. J. Comput. Chem. 2008; 29:1693–1698. [PubMed: 18307169]

42. Maestro. Schrodinger, LLC; New York, NY, USA: 9.1, www.schrodinger.com

43. MacroModel. Schrodinger, LLC; New York, NY, USA: 9.8, www.schrodinger.com

44. SiteMap. Schrödinger, LLC; New York, NY, USA: 2.4, www.schrodinger.com

45. Bradford MM. A rapid and sensitive method for the quantitation of microgram quantities of protein utilizing the principle of protein dye binding. Anal. Biochem. 1976; 76:248–254. [PubMed: 942051]

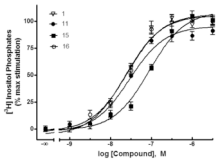

Figure 1.

Activity of native agonist **1** and alklyoxyimino derivatives **14, 15**, and **16** at the $P2Y_4$ receptor as indicated by activation of PLC in 1321N1 human astrocytoma cells stably expressing the human $P2Y_4$ receptor.

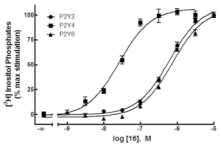

Figure 2.

Activity of compound **16** (N^4-(phenylpropoxy)-CTP) at $P2Y_2$, $P2Y_4$, and $P2Y_6$ receptors as indicated by activation of PLC in 1321N1 human astrocytoma cells stably expressing the human $P2Y_2$, $P2Y_4$, or $P2Y_6$ receptor. The effect of **1** corresponds to 100%.

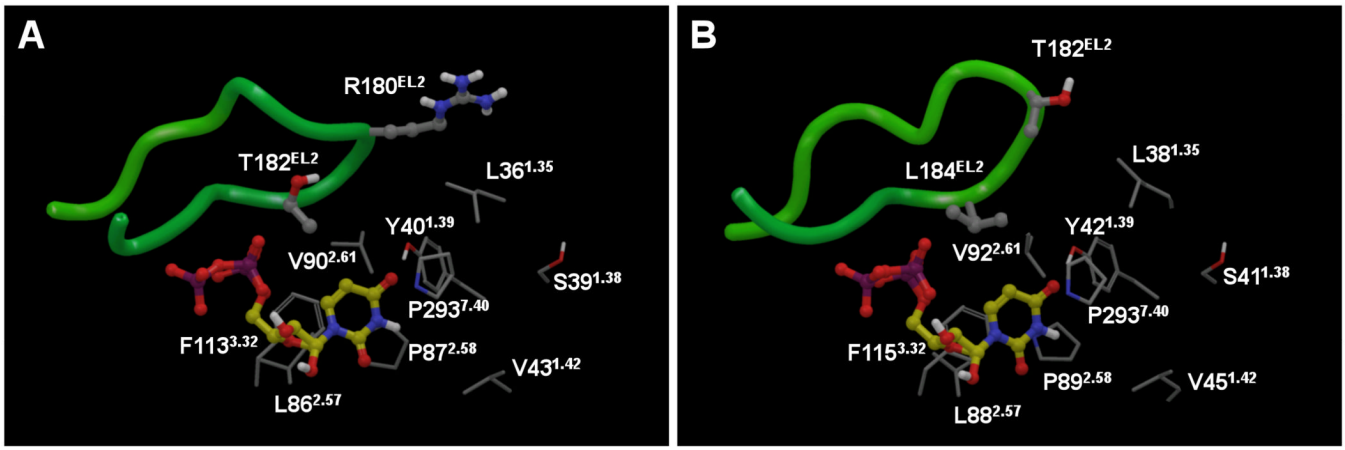

Figure 3.

Rhodopsin-based molecular models of the $P2Y_2$ and $P2Y_4$ receptors.[20] The second extracellular loop (EL2) is schematically represented as a green tube. The area that in these models would surround the N^4-substituents of the imino derivatives described in this article is completely conserved between the $P2Y_2$ and $P2Y_4$ receptor. This is in contrast with the fact that large N^4substituents are better tolerated by the $P2Y_4$ than the $P2Y_2$ receptor. Two non-conserved EL2 residues that could explain the selectivity profile of the N^4-substituents compounds according to the CXCR4 models (see Figures 5) are not positioned in a way that would allow interactions with such moieties in the rhodopsin-based models. Receptor residues are represented with gray carbons, while ligands are represented with yellow carbons. See Figure of Jacobson et al.[8] for further details on the rhodopsin-based models.

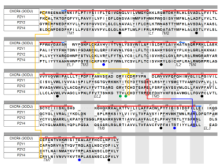

Figure 4.

Sequence alignment of $CXCR_4$, $P2Y_2$, and $P2Y_4$ receptors used for the construction of the homology models. The sequence of the $P2Y_1$ receptor, on which most of the mutagenesis studies were performed, is also shown. Green dots indicate the two non-conserved EL2 residues putatively responsible for the selectivity of compound **16** for the $P2Y_4$ receptor. Blue dots indicate the conserved cationic residues putatively responsible for coordination of the negatively charged phosphate groups of the ligands. An additional cationic residue, $Lys289^{7.36}$ of the $P2Y_4$ receptor, is proposed to interact with the α-phosphate. The cysteine residues involved in the formation of disulfide bridges are encased in a dark yellow box and connected by a dark yellow line. The glutamate and arginine residues involved in the formation of the salt bridge that putatively connects EL2 to the extracellular end of TM6, conserved also in the $P2Y_1$ receptor, are encased in a red and a blue box, respectively, and are connected by a red and blue line. The secondary structure of the template is indicated by a color-coded bar, with α-helices in red, β-strands in yellow and turns in blue. For each TM, black dots indicate the X.50 position, as defined in the GPCR indexing system. Transmembrane helices (TMs), extracellular loops (ELs) and intracellular loops (ILs) are indicated by labels. The figure was generated with MOE.[40]

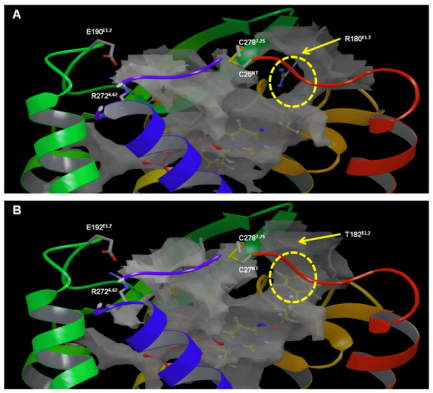

Figure 5.

Contour of interhelical cavity (in gray) of the $P2Y_2$ and $P2Y_4$ receptor deduced from the analysis of the new CXCR4 homology models. According to these models, there is only one region, indicated by a dashed yellow circle, where the cavity is significantly smaller in the $P2Y_2$ than in the $P2Y_4$ receptor. This difference is due to a non-conserved amino acid in EL2, which is a threonine (Thr182) in the $P2Y_4$ receptor and a bulkier arginine (Arg180) in the $P2Y_2$ receptor. Of note, an arginine residue is present at the corresponding position of the CXCR4 receptor (Arg183). The orientation of Arg180 in our model of the $P2Y_2$ receptor follows the orientation of Arg183 in the crystal structure of the CXCR4 receptor. The disulfide bridge that putatively links the N-terminus with EL3 and the salt bridge that putatively links TM6 with EL2 are shown. The disulfide bridge that links TM3 with EL2 is not clearly visible because it is obscured by the interhelical cavity. Compounds **11** and **16** are shown within the pockets of the $P2Y_2$ and $P2Y_4$ receptors, respectively. The backbone of the receptor is schematically represented as a ribbon colored with a continuum spectrum going from red, at the N-terminus, to purple, at the C-terminus. For convenience, TM7 is not shown.

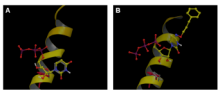

Figure 6.
Previously published rhodopsin-based model (Panel A, in complex with **1**) and new CXCR4-based model of the $P2Y_4$ receptor (Panel B, in complex with **16**). One residue of the CXCR4 receptor ($Tyr116^{3.32}$, in red) was key to deduce the putative rotameric state of the corresponding residue in the $P2Y_2$ and $P2Y_4$ receptors ($Phe113^{3.32}$ for $P2Y_2$ and $Phe115^{3.32}$ for $P2Y_4$, in gray) in the new models. The CXCR4-based rotameric state of $Phe^{3.32}$ caused a significant change of the ligand binding mode with respect to the previously published one. The backbone of TM3 is schematically represented as a yellow ribbon.

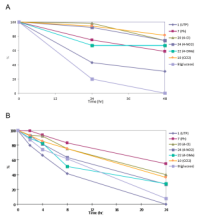

Figure 7.

A) Time-course of the hydrolysis of various nucleotides incubated at 37°C and pH 1.5. The assays were started with 0.2 mg/mL of the compound. Concentration of analogues in the medium was determined using HPLC analysis of aliquots. Data are expressed as percent of the initial peak. B) Time-course of the degradation of various nucleotides in the presence of membranes of 1321N1 astrocytoma cells. The cells were homogenized and the nuclear fraction was removed by centrifugation. The resultant pellets were suspended in Tris buffer (pH 7.4). The membrane was diluted with Dulbecco's PBS (pH 7.4) and homogenized before use for the stability check. The final protein concentration was 14.9 μg/mL. The assays were started with 0.2 mg/mL compound. Concentrations of molecules were analyzed using HPLC. Data are expressed as percent of initial peak.

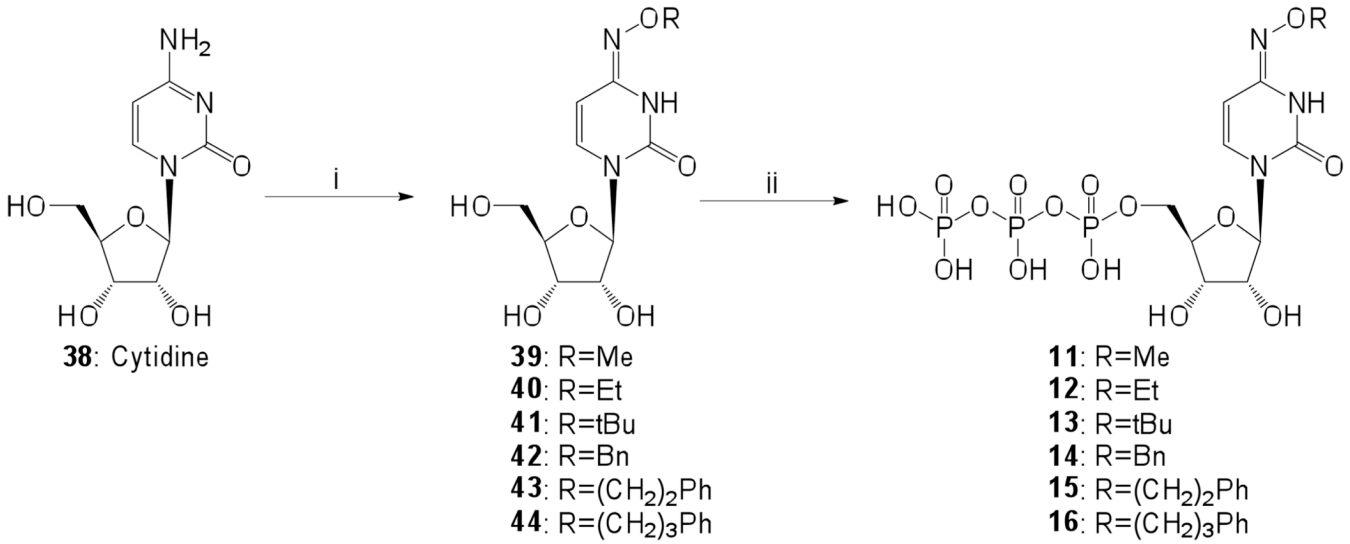

Scheme 1.

Synthesis of alkoxyimino derivatives. Reagents and conditions: i) $RONH_2$, pyridine, 100°C, overnight; ii) a) Proton Sponge, $POCl_3$, $PO(OMe)_3$, 0°C, 3 h, b) Bu_3N, tributylammonium pyrophosphate, 0,°C, 10 min, c) triethylammonium bicarbonate aq., rt, 30 min.

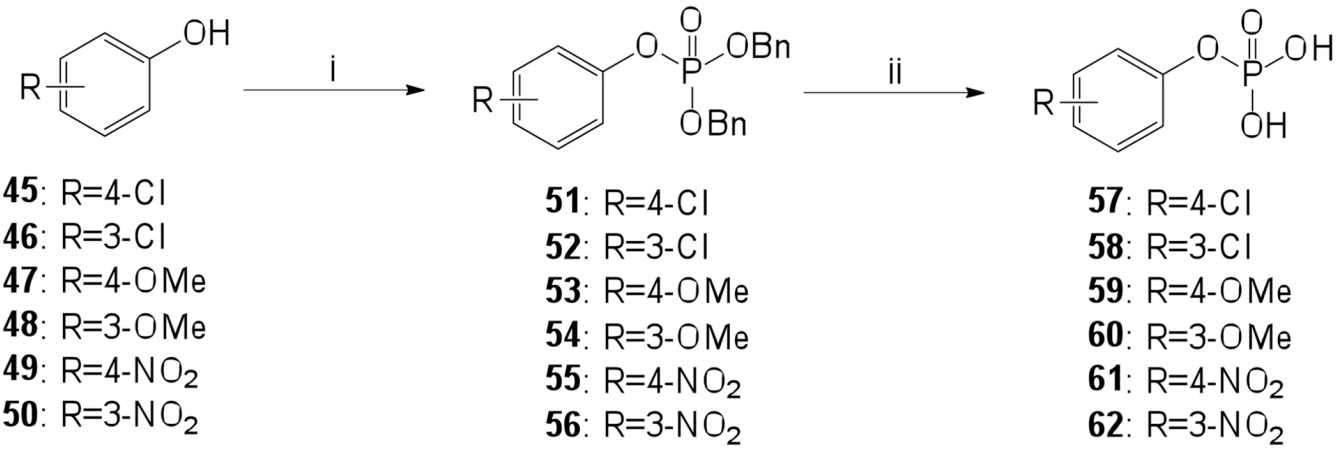

Scheme 2.

Synthesis of aryl phosphates. Reagents and conditions: i) CBr_4, iPr_2NEt, dibenzyl phosphite, MeCN, rt, 2 h; ii) TMS-Br, CH_2Cl_2, rt, 1.5 h.

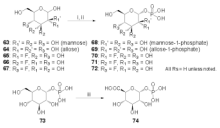

Scheme 3.

Synthesis of sugar-1-phosphates. Reagents and conditions: i) Ac_2O, NaOAc, 5 h, 110°C; ii) H_3PO_4, 50°C, 3 h; iii) TEMPO, H_2O, NaOH, NaOCl, 0°C.

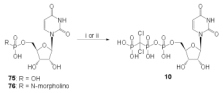

Scheme 4.

Synthesis of β, γ-dichloromethylene-UTP **10**. Reagents and conditions: from **75**, i) a) DIC, DMF, rt, 3 h; b) $PO(OH)_2CCl_2PO(OH)_2$, $MgCl_2$, DMF, rt, overnight; from **76**, ii) $PO(OH)_2CCl_2PO(OH)_2$, DMF, rt, 2 weeks.

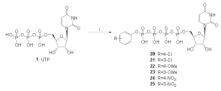

Scheme 5.

Synthesis of Up_4-δ-phenyl ester derivatives. Reagents and conditions: i) a) DIC, DMF, rt, 3 h; b) aryl-1-phosphate, $MgCl_2$, DMF, rt, overnight.

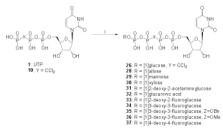

Scheme 6.

Synthesis of Up_4-δ-sugar derivatives. Reagent and condition: i) a) DIC or DCC, DMF, rt, 3 h; b) sugar-1-phosphate, $MgCl_2$, DMF, rt, 2 h to overnight. Unless noted, Y = O.

$P2Y_2/P2Y_4$ Receptor Agonists (EC_{50} at $P2Y_2/P2Y_4$, μM)

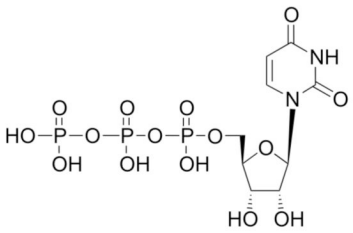

1 (0.060/0.090)

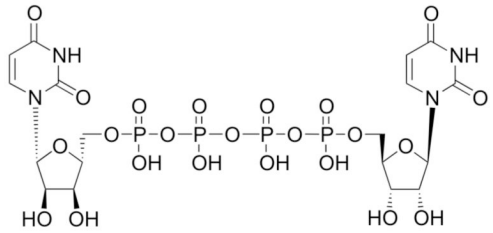

2 (1.31/0.87)

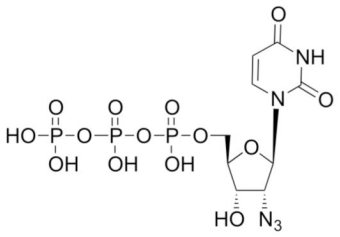

3 (5.0/1.1)

Selective $P2Y_2$ Receptor Agonists (EC_{50}, μM)

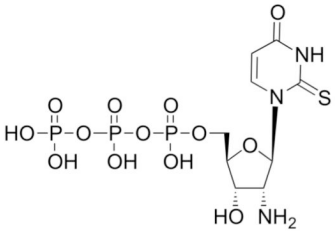

4 (0.008)

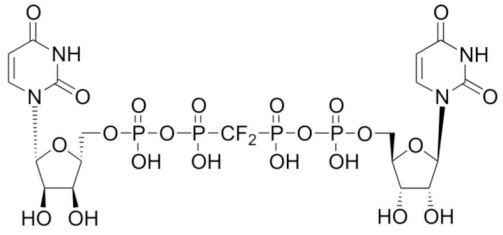

5 (2.27)

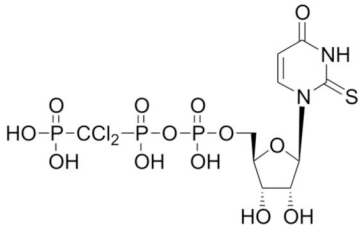

6 (2.51)

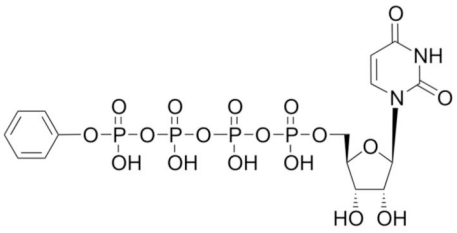

7 (1.89)

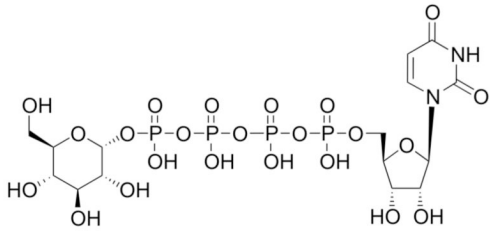

8 (0.30)

Chart 1.

Structures and potencies of prototypical agonist ligands for studying $P2Y_2$ and $P2Y_4$ receptors.

Table 1

Relative potencies of **1** and its analogues for activation of the human $P2Y_2$, $P2Y_4$ and $P2Y_6$ receptors. Unless noted: R = H; X, Y = O; and Z = O.

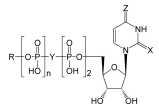

Compound	Modification	Structure	EC_{50}, nM[a]		
			hP2Y$_2$	**hP2Y$_4$**	**hP2Y$_6$**
TRIPHOSPHATES (n = 1)					
1[b]	(= UTP)		55 ± 4	80 ± 8	>10,000[d]
6[b]	2-thio-β,γ-CCl_2-UTP	X = S, Y=CCl_2	2510 ± 650	NE	NE
9[b]	2-thio-UTP	X = S	35 ± 4	350 ± 100	~1500
10[b]	β,γ- CCl_2-UTP	Y=CCl_2	9600 ± 2100	NE	≤50% at 10 μM
11	N^4-OMe-CTP	Z = *N*-OCH_3	28 ± 4	25 ± 3	130 ± 21
12	N^4-OEt-CTP	Z = *N*-OCH_2CH_3	817 ± 93	210 ± 79	877 ± 50
13	N^4-OtBu-CTP	Z = *N*-$OC(CH_3)_3$	1500 ± 240	2110 ± 680	≤50% at 10 μM
14	N^4-OBn-CTP	Z = *N*-OCH_2Ph	620 ± 75	97 ± 14	230 ± 37
15	N^4-OEtPh-CTP	Z = *N*-$O(CH_2)_2Ph$	1200 ± 270	73 ± 17	1210 ± 220
16	N^4-OPrPh-CTP	Z = *N*-$O(CH_2)_3Ph$	640 ± 147	23 ± 4	740 ± 29
TETRAPHOSPHATES (n = 2)					
17[b]	Up_4		3900 ± 1200	7300 ± 1600	7600 ± 1100
18[b]	Up_4-OMe	R = CH_3	4000 ± 510	2700 ± 430	>10,000[d]
19[b]	Up_4-$O(CH_2)_2CN$	R = $(CH_2)_2CN$	1700 ± 220	1960 ± 530	>10,000[d]
7	Up_4-OC_6H_5	R = 	2760 ± 630	NE	NE

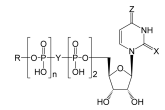

Compound	Modification	Structure	EC_{50}, nM[a]		
			$hP2Y_2$	$hP2Y_4$	$hP2Y_6$
20	Up_4-OC_6H_4(4-Cl)	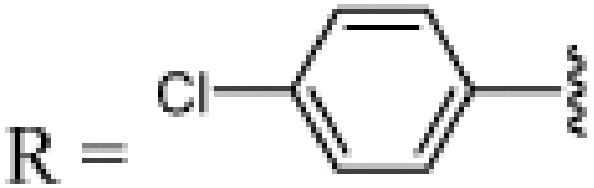	6600 ± 1600	c	c
21	Up_4-OC_6H_4(3-Cl)	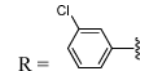	840 ± 50	NE	3690 ± 750
22	Up_4-OC_6H_4(4-OMe)	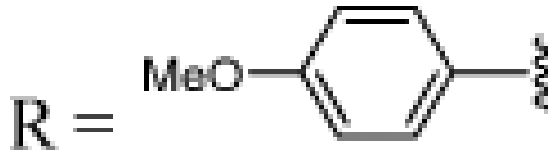	≤50% at 10 μM	≤50% at 10 μM	≤50% at 10 μM
23	Up_4-OC_6H_4(3-OMe)	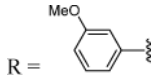	≤50% at 10 μM	NE	≤50% at 10 μM
24	Up_4-OC_6H_4(4-NO_2)	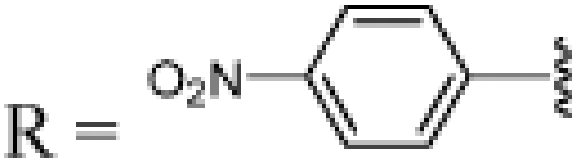	4850 ± 1000	≤50% at 10 μM	≤50% at 10 μM
25	Up_4-OC_6H_4(3-NO_2)	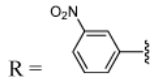	3330 ± 620	2540 ± 460	≤50% at 10 μM
TETRAPHOSPHATE SUGAR DERIVATIVES (n = 2)					
2[b]	Up_4U	R = [5]uridine	210 ± 30	130 ± 10	1160 ± 420
8[b]	Up_4-[1]glucose	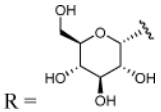	300 ± 130	2060 ± 180	7830 ± 170

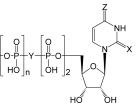

Compound	Modification	Structure	EC_{50}, nM[a]		
			hP2Y$_2$	**hP2Y$_4$**	**hP2Y$_6$**
26	β,γ-dichloromethylene-Up$_4$-[1]glucose	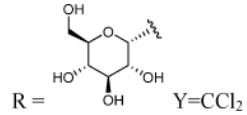	≤50% at 10 μM	NE	NE
27[b]	Up$_4$-[1]galactose	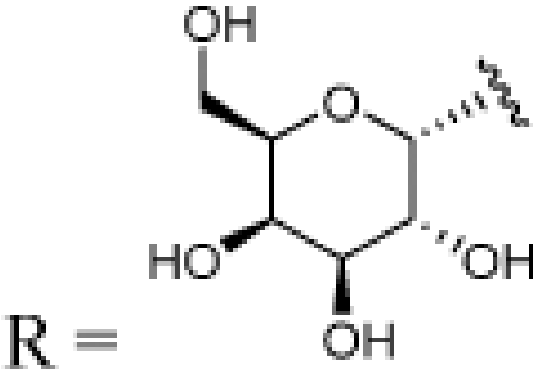	940 ± 120	1770 ± 410	8190 ± 730
28	Up$_4$-[1]allose	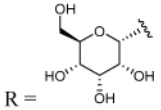	770 ± 220	183 ± 9	1170 ± 130
29	Up$_4$-[1]mannose	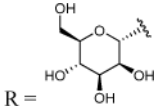	3720 ± 1140	4480 ± 620	12,100 ± 2450

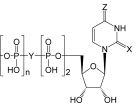

Compound	Modification	Structure	EC_{50}, nM[a]		
			hP2Y$_2$	**hP2Y$_4$**	**hP2Y$_6$**
30	Up_4-[1]xylose	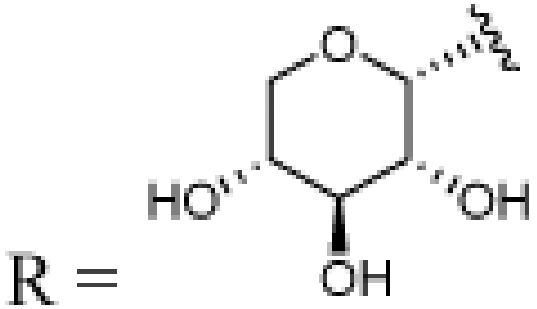	2770 ± 560	620 ± 30	4900 ± 660
31	Up_4-[1]2'-deoxy-2'-acetamidoglucose	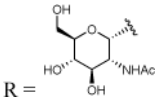	1890 ± 400	910 ± 100	5460 ± 860
32	Up_4-[1]glucuronic acid	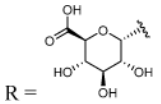	490 ± 44	227 ± 88	1650 ± 340
33	Up_4-[1]2′-deoxy-2′-fluoroglucose	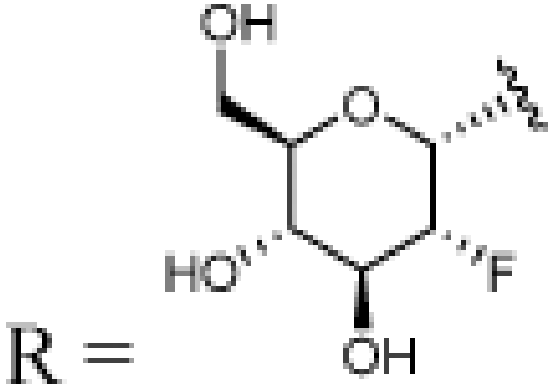	≤50% at 10 μM	≤50% at 10 μM	≤50% at 10 μM

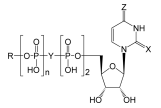

Compound	Modification	Structure	EC_{50}, nM[a]		
			$hP2Y_2$	$hP2Y_4$	$hP2Y_6$
34	Up_4-[1]3′-deoxy-3′-fluoroglucose	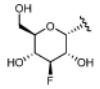	710 ± 120	62 ± 19	950 ± 150
35	N^4-OBn-Cp_4-[1]3′-deoxy-3′-fluoroglucose	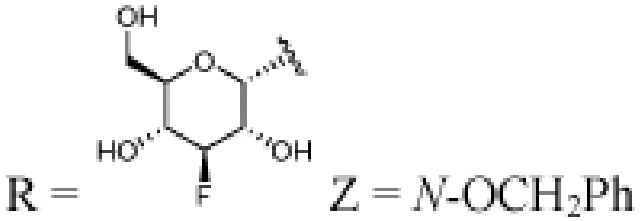	2640 ± 588	670 ± 100	7510 ± 240
36	N^4-OMe-Cp_4-[1]3′-deoxy-3′-fluoroglucose	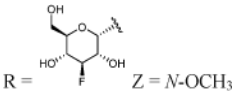	500 ± 62	310 ± 13	1440 ± 280
37	Up_4-[1]4′-deoxy-4′-fluoroglucose	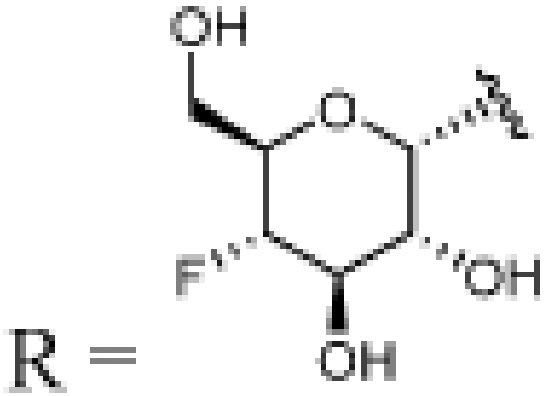	620 ± 220	220 ± 30	1640 ± 140

[a] Agonist potencies reflect stimulation of PLC in 1321N1 human astrocytoma cells stably expressing the human $P2Y_2$, $P2Y_4$, or $P2Y_6$ receptor. Potencies are presented in the form of EC_{50} values, which represent the concentration of agonist at which 50% of the maximal effect is achieved. These values were determined using a four-parameter logistic equation and the GraphPad software package (GraphPad, San Diego, CA). The results are presented as mean ± standard error and are the average of three to six different experiments with each molecule.

[b] Agonist potencies for compounds **2, 6, 8, 9, 18**, and **19** were from published reports.[8,13] Compounds **1, 7, 10, 17**, and **27** were reported in Ko et al.[13] but reassayed in this study.

J Med Chem. Author manuscript; available in PMC 2012 June 23.

[c] Not determined.

[d] ≤50% effect at 10 μM. Values of >10 μM were determined by extrapolation.

NE - no effect at 10 μM.